Release of VAMP5-positive extracellular vesicles from specialized domains of retinal Müller cells *in vivo*

Short: Extracellular vesicles from retinal Müller cells

Valerie Demais[1§], Anne Pohl[2,3§], Kirsten A. Wunderlich[2], Anna M. Pfaller[2], Lew Kaplan[2], Amelie Barthélémy[4], Robin Dittrich[5], Berta Puig[6], Bernd Giebel[5], Stefanie M. Hauck[7], Frank W. Pfrieger[1,4]*, Antje Grosche[2]*

[1] Plateforme Imagerie In Vitro, CNRS UAR 3156, Neuropôle, University of Strasbourg, 67000 Strasbourg, France.

[2] Department of Physiological Genomics, BioMedical Center BMC, Ludwig-Maximilian University, 82152 Planegg-Martinsried, Germany.

[3] Institute of Human Genetics, University of Regensburg, 93053, Regensburg, Germany.

[4] Centre National de la Recherche Scientifique, Université de Strasbourg, Institut des Neurosciences Cellulaires et Intégratives, 67000 Strasbourg, France.

[5] Institute for Transfusion Medicine, University Hospital Essen, University of Duisburg-Essen, 45147 Essen, Germany.

[6] Neurology Department, Experimental Research in Stroke and Inflammation (ERSI), University Medical Center Hamburg-Eppendorf, 20246 Hamburg, Germany.

[7] Metabolomics and Proteomics Core and Research Unit Protein Science, Helmholtz-Zentrum München, 80939 München, Germany.

[§]Equally contributing first authors; *Corresponding authors

Abstract

Cell-cell interactions in the central nervous system (CNS) are based on the release of molecules mediating signal exchange and providing structural and trophic support through vesicular exocytosis and the formation of extracellular vesicles (EVs). The specific mechanisms employed by each cell type in the brain are incompletely understood. Here, we explored the means of communication used by Müller cells, a type of glial cells in the retina, which forms part of the CNS. Using immunohistochemical, electron microscopic, and molecular analyses, we provide evidence for the release of distinct EVs from highly specialized domains of Müller cells in retinae from adult mice *in vivo*. We identify VAMP5 as a Müller cell-specific SNARE component that is part of EVs and responsive to ischemia, and we reveal differences between the secretomes of affinity-purified Müller cells and neurons *in vitro*. Our findings suggest EV-based communication as an important mediator of cellular interactions in the retina.

Keywords: neuroglia, exosomes, tetraspanin, gliosis, SNARE complex, secretome, vitreous body

Word Count: 12645

Introduction

Glial cells control the development (Araujo et al., 2019; Lago-Baldaia et al., 2020; Tan et al., 2021) and function (García-Cáceres et al., 2019; Kofuji and Araque, 2021; Nave and Werner, 2021) of neurons and they influence the outcome of pathologic conditions due to disease or injury (Kim et al., 2020; Linnerbauer et al., 2020; Patel et al., 2019; Raiders et al., 2021; Wilton et al., 2019; Wilton and Stevens, 2020). During the last years, much has been learned

about glia-neuron interactions: neurons and different types of glial cells communicate via intercellular contacts and via the release of molecules fulfilling multiple functions that range from structural, energy and trophic support to cell signaling (Giaume et al., 2021; Hillen et al., 2018; Illes et al., 2019; Jha and Morrison, 2020; Seifert and Steinhäuser, 2018; Shen et al., 2017; Sultan et al., 2015). Molecules of the secretome that are contained in intracellular vesicles can be released directly into the extracellular space following fusion of the vesicular membrane with the plasma membrane (Fiacco and McCarthy, 2018; Murat and García-Cáceres, 2021; Savtchouk and Volterra, 2018; Vardjan et al., 2019). Alternatively, they can be released as molecular assemblies contained in extracellular vesicles (EVs) harboring a context- and cell type-specific host of proteins, lipids, and nucleic acids (Kalluri and LeBleu, 2020; Mathieu et al., 2019; Pfrieger and Vitale, 2018; Pistono et al., 2020; Théry et al., 2018; van Niel et al., 2022; Yates et al., 2022). EVs have been discussed as potential means of cell-cell communication in the normal and diseased central nervous system (CNS) (Aires et al., 2021; Budnik et al., 2016; Li et al., 2019; Liu et al., 2020; Lizarraga-Valderrama and Sheridan, 2021; Pascual et al., 2020; Schnatz et al., 2021; Sharma et al., 2013; You and Ikezu, 2019), but knowledge about their presence, composition, and origin in nervous tissues *in vivo* is still incomplete (Brenna et al., 2021). Here, we explored possible mechanisms of glial communication in the CNS using the retina as model tissue. We focus on Müller cells, a prominent type of retinal glia that impacts retinal development and function by diverse mechanisms (Reichenbach and Bringmann, 2020). Previous studies suggested that these cells employ vesicular release of molecules (Slezak et al., 2012; Wagner et al., 2017), but the full range of their intercellular communication capacity is unknown. Our findings suggest that Müller cells release EVs from their endfeet facing the vitreous body and their microvilli surrounding photoreceptor segments. We show that Müller cell-derived EVs have a characteristic protein composition that differs substantially from those secreted by neurons.

Moreover, we uncover that vesicle-associated membrane protein 5 (VAMP5), a component of soluble N-ethylmaleimide-sensitive factor attachment proteins receptor (SNARE) complexes, is specifically expressed by retinal Müller cells and contained in a subset of their EVs.

Materials and Methods

Animals

All experiments were performed with adult C57BL/6J mice in accordance with the European Community Council Directive 2010/63/EU and the ARVO Statement for the Use of Animals in Ophthalmic and Vision Research. Animals were housed in a 12h light/dark cycle with ~400 lux with *ad libitum* access to drinking water and food.

Transient retinal ischemia

The protocols for induction of transient retinal ischemia were approved by the local Bavarian authorities (55.2 DMS-2532-2-182, Germany). Ischemia was induced in one eye of 8-weeks-old male and female mice using the high intraocular pressure (HIOP) method (Pannicke et al., 2014; Wagner et al., 2016). The untreated contralateral eye served as internal control. This approach reduced the number of animals used in these experiments as demanded by the 3R rules. Anesthesia was induced by intraperitoneal injection of ketamine (100 mg/kg body weight; Ratiopharm, Ulm, Germany) and xylazine (5 mg/kg; Bayer Vital, Leverkusen, Germany). Pupillary dilation was induced by atropine sulfate (100 mg/kg; Braun, Melsungen, Germany). The anterior chamber of the test eye was cannulated from the pars plana with a 30-gauge infusion needle connected to a bottle containing saline (0.9% NaCl). The intraocular pressure was increased to 160 mm Hg by elevating the bottle for 90 min. After

removing the needle, animals were returned to cages and sacrificed after different periods of time for tissue analyses using carbon dioxide.

Cell isolation

Specific retinal cell types were enriched from adult mice as described previously using immunomagnetic separation (Grosche et al., 2016; Pauly et al., 2019). Briefly, retinae were treated with papain (0.2 mg/ml; Roche Molecular Biochemicals) for 30 min at 37°C in the dark in calcium- and magnesium-free extracellular solution (140 mM NaCl, 3 mM KCl, 10 mM HEPES, 11 mM glucose, pH 7.4). After several rinses and 4 min of incubation with DNase I (200 U/ml), retinae were triturated in extracellular solution with 1 mM $MgCl_2$ and 2 mM $CaCl_2$ added. The retinal cell suspension was subsequently incubated with CD11b- and CD31-binding microbeads to deplete microglia and vascular cells, respectively, according to the manufacturer's instructions (Miltenyi Biotec, Bergisch Gladbach, Germany). The respective binding cells were depleted from the retinal suspension using large cell (LS)-columns, prior to Müller cell enrichment. To purify Müller cells, the cell suspension was incubated in extracellular solution containing biotinylated anti-CD29 (0.1 mg/ml, Miltenyi Biotec) for 15 min at 4°C. Cells were washed in extracellular solution, spun down, resuspended in the presence of anti-biotin MicroBeads (1:5; Miltenyi Biotec) and incubated for 15 min at 4°C. After washing, CD29-positive Müller cells were enriched using LS columns according to the manufacturer's instructions (Miltenyi Biotec). Cells in the flow-through of the last sorting step – depleted of microglia, vascular cells, and Müller cells – were considered as mixed neuronal population.

Immunohistochemical and -cytochemical staining

Enucleated eyes were immersion-fixed (4% paraformaldehyde for 2 h), washed with phosphate-buffered saline (PBS), cryoprotected in sucrose, embedded in Tissue-Tek® O.C.T. compound (Sakura Finetek, Staufen, Germany), and cut in 20 µm sections using a cryostat. Retinal sections were permeabilized (0.3% Triton X-100 plus 1.0% DMSO in PBS) and blocked (5% normal goat serum with 0.3% Triton X-100 and 1.0% DMSO in PBS) for 2h at room temperature (RT). Cultured cells were fixed (4% paraformaldehyde for 15 min), washed with phosphate-buffered saline (PBS), permeabilized (0.3% Triton X-100 plus 1.0% DMSO in PBS) and blocked (5% normal goat serum with 0.3% Triton X-100 and 1.0% DMSO in PBS; 30 min at RT). Primary antibodies (Supplementary Table 1) in bovine serum albumine (1% in PBS) were incubated overnight at 4°C. Sections or fixed cultured cells were washed (1% BSA) and incubated with secondary antibodies (2h at RT; 1% BSA). Cell nuclei were labeled with DAPI (1:1000; Life Technologies). Samples were mounted in Aqua-Poly/Mount (Polysciences, Hirschberg an der Bergstrasse, Germany). Control experiments without primary antibodies showed no unspecific labeling except for the goat-anti-mouse secondary antibody that labeled blood vessels (not shown). Images of stained sections and cells were acquired with a custom-made VisiScope CSU-X1 confocal system (Visitron Systems, Puchheim, Germany) equipped with a high-resolution sCMOS camera (PCO AG, Kehlheim, Germany). For super resolution microscopy fixed retinal sections were permeabilized with Triton X-100 (0.5 % in 2% BSA in PBS) for 2h before incubation with primary antibodies in blocking solution (overnight at 4°C). After washing with PBS, sections were incubated with secondary antibodies (Abberior Star) and DAPI for 2h in blocking solution at RT, subsequently washed with PBS, and briefly rinsed with distilled water before being mounted with ProLong Gold antifade reagent (Invitrogen, Life Technologies). Stimulated emission depletion (STED) microscopy was performed at the Core Facility

Bioimaging of the Biomedical Center of the LMU München with an inverted Leica SP8 STED X WLL microscope using appropriate lasers for fluorophore excitation (405 nm; pulsed white light laser 470 – 670 nm). Images were acquired with a 93x/1.3 NA glycerol immersion objective, pixel size set to 23 nm. The following spectral settings were used: DAPI (excitation: 405 nm; emission: 415 – 450 nm; PMT), AbberiorStar 580 (580 nm; 590 – 620 nm; HyD; depletion laser: pulsed 775 nm, at 12% intensity), AbberiorStar 635P (635 nm; 645 – 702 nm; HyD; depletion laser: pulsed 775 nm, at 12% intensity). Recording of color channels was performed sequentially to avoid bleed-through. Image brightness and contrast were adjusted with the open source software FIJI (Schindelin et al., 2012).

Immunoblotting of proteins from affinity-purified cells

Pellets of enriched cell populations from pooled pairs of mouse eyes were redissolved in reducing RIPA buffer, denatured and sonicated. Protein amounts were quantified using the RC DC Protein Assay (BioRad, Feldkirchen, Germany) according to the manufactures instructions. Equal amounts of protein per sample were loaded to compare levels of selected VAMPs in cells. Samples were separated on a 12% SDS-PAGE and immunodetection of proteins was performed as described (Schäfer et al., 2017) using primary and secondary antibodies (Supplementary Table 1) diluted in blocking solution (5% BSA in TBST). Blots were developed with WesternSure PREMIUM Chemiluminescent Substrate (LI-COR, Bad Homburg, Germany).

Test of VAMP5 antibody specificity by immunoprecipitation

Retinae were dissected from adult mice and lysed mechanically and chemically using RIPA. The protein concentration was determined by the RC DC Protein Assay (BioRad). For immunoprecipitation, to each sample batch (1 mg of total retinal extract, four mouse retinae

each), 5 µg of anti-VAMP5 antibody or a rabbit IgG-control antibody was added (Supplementary Table 1) and the antibody-lysate mix was incubated on the rotator at 4 °C for four hours. For affinity purification, 25 µl of Protein G Sepharose® (Merck, Darmstadt, Germany) were were resuspended three times in TBS (0.5% NP40) and then centrifuged at 2,000 g for five minutes. Beads were added to the antibody-lysate mix and incubated on the rotator at 4 °C overnight. The complexes formed by antibody, antigen, and Protein G Sepharose® were pelleted (4,000 g for 5 min) two times, and washed in TBS. Proteins were eluted in Laemmli buffer for 10 minutes at 37 °C and spun down at 4,000g. Supernatant was collected and stored at -20 °C for analysis by mass spectrometry.

Transcript profiling of affinity-purified cells by RNAseq

Total RNA was isolated from cell pellets after immunomagnetic cell separation using the PureLink® RNA Micro Scale Kit (Thermo Fisher Scientific, Schwerte, Germany). Validation of RNA integrity and quantification of RNA concentrations were performed using the Agilent RNA 6000 Pico chip analyser according to the manufacturer's instructions (Agilent Technologies, Waldbronn, Germany). Enrichment of mRNA, library preparation (Nextera XT, Clontech), quantification (KAPA Library Quantification Kit Illumina, Kapa Biosystems, Inc., Woburn, MA, USA) and sequencing on an Illumina platform (NextSeq 500 High Output Kit v2; 150 cycles) were performed at the service facility of the KFB Center of Excellence for Fluorescent Bioanalytics (Regensburg, Germany; www.kfb-regensburg.de). After de-multiplexing, at least 20 million reads per sample were detected. Quality control (QC) of the reads and quantification of transcript abundance were performed with the Tuxedo suite software (Langmead et al., 2009; Trapnell et al., 2009). To this end, the cutadapt routine was used to remove adapter sequences (Martin, 2011) and several QC measures were obtained with the fastqc routine. Next, the trimmed reads were aligned to the reference

genome/transcriptome (GRCm38) with HISAT2 (Kim et al., 2015). Transcript abundance was estimated with the stringtie routine (Pertea et al., 2015) and expressed as fragments per kilobase pairs of transcripts per million reads (fragments per kilobase million, FPKM).

Quantitative reverse-transcriptase polymerase chain reaction (qRT-PCR) of affinity-purified cells

Total RNA was isolated from pelleted cells after immunomagnetic separation using the PureLink® RNA Micro Scale Kit (Thermo Fisher Scientific, Schwerte, Germany). An on-column DNase digestion step (PureLink® DNase mixture, Thermo Fisher Scientific, for 20 min at RT) was included to remove genomic DNA (Roche Molecular Systems, Mannheim, Germany). RNA integrity was validated using the Agilent RNA 6000 Pico Assay according to the manufacturer's instructions (Agilent Technologies, Waldbronn, Germany). First-strand cDNAs from the total RNA purified from each cell population were synthesized using the RevertAid H Minus First-Strand cDNA Synthesis Kit (Fermentas by Thermo Fisher Scientific, Schwerte, Germany). Primers were designed using the Universal ProbeLibrary Assay Design Center (Roche, Supplementary Table 2) and transcript levels of candidate genes were measured by qRT-PCR using the TaqMan hPSC Scorecard™ Panel (384 well, ViiA7, Life Technologies, Darmstadt, Germany) according to the manufacturer’s guidelines.

TUNEL staining

Affinity-purified cells were cultured on coverslips, fixed (4% PFA, 15 min at RT) and permeabilized (0.25% Triton® X-100 in PBS, 20 min at RT). Afterwards, the solution was removed by washing twice with de-ionized water. The cells were then pretreated for 10 min at RT in TdT reaction buffer (Click-iT™ Plus TUNEL Assay, Alexa Fluor™ 594 dye, ThermoFisher Scientific, Schwerte, Germany), before the enzyme mix was added and

incubated for 60 min at 37◦C. After two washes in 3% BSA/PBS (2 min each), the Click iT® reaction cocktail was added and incubated for another 30 min at RT. A subsequent staining for the Müller cell marker glutamine synthetase (GLUL) and DAPI co-staining was performed as described in the section 'Immunohistochemical and -cytochemical staining', after cover slips were washed two times (3% BSA/PBS for 5 min at RT). Images of cells were taken with custom-made VisiScope CSU-X1 confocal system (Visitron Systems, Puchheim, Germany).

EV preparation from primary cultures of affinity-purified cells

Approximately 600,000 and 300,000 immunomagnetically sorted neurons and Müller cells, respectively, were seeded into individual wells of a 48-well-plate with 400 µl DMEM-F12 GlutaMax supplemented with Gibco™ Antibiotic-Antimycotic (1:100; Thermo Fischer Scientific) and NeuroBrews (1:50; Miltenyi Biotec). Small samples of cells were fixed and air-dried onto glass slides to control for cell purity by immunocytochemical staining of GLUL. After 48h to 60h, conditioned media (CM) were collected from cells and preserved for subsequent preparation of released material. In parallel, cells were harvested from the culture plates, pelleted by centrifugation, and immediately lysed in hot SDS (0.1 % in distilled water) for mass spectrometry or in RIPA buffer for immunoblotting and frozen at -80°C until further processing. CM were cleared by several centrifugation steps with increasing speed and duration (600 g for 10 min; 2,000 g for 30 min; 10,000 g for 45 min) and subjected to immunomagnetic separation of material positive for the surface markers CD63 and CD9 (Miltenyi) following the manufacturer's instructions. Affinity-purified material containing EVs was characterized at the molecular and structural level according to the MISEV2018 guidelines (Théry et al., 2018). For protein analyses, proteins in material subjected to immunomagnetic separation from CM were directly eluted and lysed from the µ-

columns still in the magnet either with hot SDS (0.1 %) in distilled water for mass spectrometry or in RIPA buffer for immunoblotting. The material in the flow-through of the washing steps was pelleted by ultracentrifugation (at 100,000 g for 2h; Optima MAX -XP Ultracentrifuge from Beckman Coulter equipped with a TLA55 rotor) before lysis. Each lysed fraction was frozen at -80°C until further use.

Immunoblotting of proteins from cultured cells and their secreted EVs

EV-containing samples from CM and respective cell lysates were diluted in Laemmli sample buffer and separated using SDS-PAGE (15%). Semidry blotting was performed using TRISbase (2.5 mM with 192 % glycine and 20% methanol) as transfer buffer. PVDF membranes were blocked and incubated with primary and secondary antibodies using non-fat dry milk (5% in TBS with 0.1% Tween 20). Blots were developed with Clarity MaxTM Western ECL substrate (Bio-Rad Medical Diagnostics GmbH, Dreieich, Germany).

Nanoparticle tracking analysis

EV-containing samples from CM were charactized by nanoparticle tracking analysis (NTA) allowing for particle quantification and average size estimation (Dragovic et al., 2011; Sokolova et al., 2011). The ZetaViewTM platform (ParticleMetrix, Meerbusch, Germany) was calibrated with polystyrene beads of 100 nm diameter (Thermo Fisher). Analyses were performed exactly as described (Görgens et al., 2019). Briefly, with 5 repetitions, videos were recorded at all 11 positions. The machine's sensitivity was set to 75, the shutter to 75 and the framerate to 30.

Quantitative proteomics - LC-MSMS analysis, label-free quantification and data analysis

Proteins were proteolysed with LysC and trypsin with filter-aided sample preparation procedure (FASP) as described (Grosche et al., 2016; Wiśniewski et al., 2009). Acidified eluted peptides were analyzed on a Q Exactive HF-X mass spectrometer (Thermo Fisher Scientific) online coupled to a UItimate 3000 RSLC nano-HPLC (Dionex). Samples were automatically injected and loaded onto the C18 trap cartridge and after 5 min eluted and separated on the C18 analytical column (Acquity UPLC M-Class HSS T3 Column, 1.8 µm, 75 µm x 250 mm; Waters) by a 95 min non-linear acetonitrile gradient at a flow rate of 250 nl/min. MS spectra were recorded at a resolution of 60,000 with an automatic gain control (AGC) target of 3 x 10e6 and a maximum injection time of 30 ms from 300 to 1,500 m/z. From the MS scan, the 15 most abundant peptide ions were selected for fragmentation via HCD with a normalized collision energy of 28, an isolation window of 1.6 m/z, and a dynamic exclusion of 30 s. MS/MS spectra were recorded at a resolution of 15,000 with a AGC target of 10e5 and a maximum injection time of 50 ms. Unassigned charges and charges of +1 and >+8 were excluded from precursor selection. Acquired raw data were analyzed in the Proteome Discoverer 2.4 SP1 software (Thermo Fisher Scientific; version 2.4.1.15) for peptide and protein identification via a database search (Sequest HT search engine) against the SwissProt Mouse database (Release 2020_02, 17061 sequences), considering full tryptic specificity, allowing for up to one missed tryptic cleavage site, precursor mass tolerance 10 ppm, fragment mass tolerance 0.02 Da. Carbamidomethylation of cysteine was set as a static modification. Dynamic modifications included deamidation of asparagine and glutamine, oxidation of methionine, and a combination of methionine loss with acetylation on protein N-terminus. The Percolator algorithm (Käll et al., 2007) was used to validate peptide spectrum matches and peptides. Only top-scoring identifications for each spectrum were accepted, additionally satisfying a false discovery rate < 1% (high confidence). The final list of proteins

satisfying the strict parsimony principle included only protein groups passing an additional protein confidence false discovery rate < 5% (target/decoy concatenated search validation). Quantification of proteins, after precursor recalibration, was based on intensity values (at RT apex) for all unique peptides per protein. Peptide abundance values were normalized on total peptide amount. The protein abundances were calculated summing the abundance values for admissible peptides. To compare proteins in EVs and lysate, the final protein ratio was calculated using median abundance values of five biological replicates each. The statistical significance of the ratio change was ascertained with ANOVA. P values are adjusted for multiple testing by Benjamini-Hochberg correction. Proteins with an adjusted P value < 0.05 were deemed significant. To generate the heatmaps using open source programming language R (Team, 2021), mass spectrometric data were first filtered to include only proteins that were detected in at least three of five biological replicates of the CD9- or C63-positive EV fractions of neurons or Müller cells. Moreover, proteins had to be enriched by 1.25 fold in the respective EV fraction compared to the lysate fraction. To generate an abundance heatmap, normalized abundance values were log2-transformed and the Manhattan distances between the samples and proteins, respectively, were calculated. Using hierarchical clustering with the ward.D2 method, we generated dendrograms that were cut in 11 clusters for the proteins and 2 clusters for the samples. The heatmap itself including annotations was created with the pheatmap package (https://cran.r-project.org/web/packages/pheatmap/index.html). The smaller 11 clusters were then combined into 4 major clusters, for which gene enrichment analysis was performed using g:Profiler (ordered query, g:SCS threshold of a p-value <0.05) (Raudvere et al., 2019). Venn diagrams were created using R (Team, 2021) with proteins showing a more than 2-fold increase in the respective CD9- or CD63-positive EV fraction compared to cell lysates prepared in parallel. Proteins were ranked based on abundance values in respective CD9- or CD63-positive EV fractions relative to values in cell lysates. To

highlight established EV markers, protein data were downloaded from the Vesiclepedia website (version 4.1) (Pathan et al., 2019) and restricted to components that were detected by at least three independent experimental approaches.

Immunogold labeling of retinae and transmission electron microscopy

Retinae were fixed (PFA 4%, glutaraldehyde 0.1% in PBS at pH 7.4 for 1h at RT), washed in PBS, incubated with saponin (0.1% in PBS for 1h), and washed with BSA (2% in PBS, five times for 10 min each). Retina were incubated overnight at 4°C with an antibody against VAMP5 (1:100), CD63 (1:50) or CD9 (1:50; 0.1% BSA in PBS). After washing (2% BSA in PBS), retinae were incubated with ultrasmall nanogold F(ab') fragments of goat anti-rabbit or goat anti-mouse (1:100, 0.1% BSA in PBS; Aurion), rinsed (0.1% BSA in PBS) and then washed in PBS and water. Gold particles were silver-enhanced using the R-Gent SE-EM kit (Aurion). For double immungold labeling, retinae were washed again several times in distilled water and phosphate buffer (PB; 0.1M NaH2PO4; pH 7.4), blocked (5% normal goat serum in PBS) and incubated overnight at 4°C with an additional antibody. After washing (5% normal goat serum in PBS), retinae were incubated with ultrasmall nanogold F(ab') fragments of goat anti-rat (1:100, 0.1% normal goat serum in PBS; Aurion). After several rinses in phosphate buffer, retina were fixed (2.5% glutaraldehyde in PB) and washed in PB and in distilled water. The second round of gold particles was silver enhanced using the R-Gent SE-EM kit (Aurion) until they showed distinct sizes from the first ones. Immunogold-labeled retinae were postfixed (0.5% OsO4 in distilled water) for 15 min. Finally, samples were dehydrated in graded ethanol series and embedded in Embed 812 (EMS). The ultrathin sections were cut with an ultramicrotome (Leica), stained with uranyl acetate [1% (w/v) in 50% ethanol], and examined by transmission electron microscopy (TEM; Hitachi H7500 equipped with an AMT Hamamatsu digital camera).

Immunogold labeling of EVs and TEM

EVs were fixed (4% PFA, 0.1% glutaraldehyde in PBS at pH 7.4 for 1h), washed (PBS), dried overnight on a glass coverslip for scanning electron microscopy (SEM) or on a formvar-carbon grid for TEM and washed (BSA 2% in PBS, five times for 10 min each). EV samples were incubated overnight at 4°C with antibodies against VAMP5 (1:100) and CD63 (1:50) or CD9 (1:50; 0.1% BSA in PBS), washed (2% BSA in PBS), and incubated for 1h with nanogold F(ab') fragments (1:100 in PBS with 0.1% BSA, Aurion) with different particle sizes and secondary antibodies (goat anti-rabbit: 40 nm for SEM and 5 nm for TEM; goat anti-mouse or goat anti-rat: 25 nm for SEM or 15 nm for TEM). After several rinses in PB, EVs were fixed in glutaraldehyde (2.5% in PB), washed in PB and postfixed in OsO_4 (0.5% in PB for 15 min). Finally, all samples were rinsed in distilled water, dehydrated in graded ethanol series, desiccated in hexamethyldisilazane, and air dried. TEM samples were stained with uranyl acetate [1% (w/v) in distilled water] and examined. SEM samples were carbon coated and examined by SEM at 15kV (Hitachi S800). Secondary electron and backscatter electron images were collected simultaneously by corresponding detectors.

Statistical analysis

Statistical analyses were performed with indicated tests using GraphPad Prism software (version 7). In figures, significance levels are indicated by asterisks (*, $p < 0.05$; **, $p < 0.01$; ***, $p < 0.001$). Whiskers in figures indicate standard error of the mean (SEM).

Results

We aimed to explore vesicle-based communication by retinal Müller cells using adult mice as experimental model. As a first step, we determined which vesicle-associated membrane

proteins (VAMPs) are expressed by retinal Müller cells using immunohistochemical staining of retinal sections. We focused on the VAMP family as these proteins are part of the SNARE complex mediating membrane fusion and thus the cellular release of molecules and vesicles (Südhof and Rothman, 2009; Urbina and Gupton, 2020).

Expression of selected VAMPs in retinal Müller cells and their post-ischemic upregulation

As shown in Fig. 1a, each member of the VAMP family showed a distinct expression pattern in the mouse retina. Notably, we observed an overlap of cellubrevin/VAMP3, myobrevin/VAMP5 and VAMP8 with the Müller cell-specific markers GLUL or retinaldehyde binding protein 1 (RLBP1). On the other hand, VAMP1, 2, 4 and 7 were present in specific retinal layers and cells that did not express glial markers (Fig. 1a). We validated these findings using independent experimental approaches (Fig.1b,c). Cell-specific transcript analyses by RNAseq and qRT-PCR using lysates of affinity-purified cells (Grosche et al., 2016; Pauly et al., 2019) corroborated our results obtained by immunohistochemical staining (Fig. 1b). Müller cells expressed *Vamp3*, *Vamp5* and *Vamp8*, whereas *Synaptobrevin/Vamp2*, a component of synapses, was enriched in neurons indicating the validity of cell-specific profiles. We also examined the presence of VAMP proteins in affinity-purified cells by immunoblotting (Fig. 1c) and its cellular distribution by immunocytochemical staining of acutely isolated Müller cells (Fig. 1d). These experiments revealed that Müller cells express VAMP3 and VAMP5 and that both VAMPs show a punctate distribution indicating their presence in vesicle-like structures (Fig. 1d). Validity of the VAMP5 antibody (Supplementary Table 1) was indicated by the observation that VAMP5-deficient mice show strongly reduced signals in immunoblots and immunohistochemical staining performed with the same antibody (Ikezawa et al., 2018).

Moreover, VAMP5 appeared as a top enriched protein in immunoprecipitated retinal lysates analysed by mass spectrometry (Supporting Data 1).

Glial cells react swiftly to injury and disease with prominent and context-specific changes in their expression profiles (Escartin et al., 2021; Pekny et al., 2016; Zamanian et al., 2012). To test whether expression of *Vamp3*, *5* and *8* in Müller cells changes during gliosis, we used an established model of transient retinal ischemia (Pannicke et al., 2014; Wagner et al., 2016). We observed several-fold increases of these glia-specific VAMPs transcripts in cells isolated from ischemic retinae compared to cells from control tissue of contralateral eyes (Fig. 2a). The increased transcript counts translated to enhanced protein levels as shown by immunohistochemical staining (Fig. 2b). Transcript levels of other members of the VAMP family were not altered. Taken together, these results showed that Müller cells express a subset of VAMPs, whose levels increase under pathologic conditions.

Presence of VAMP5 in multivesicular bodies of retinal Müller cells and in the extracellular space facing the internal and external limiting membranes *in vivo*

The unexpectedly strong expression of VAMP5 in Müller cells prompted us to focus on this member of the VAMP family and to scrutinize its subcellular distribution. Immunogold staining of retinal sections combined with TEM corroborated the presence of VAMP5 in Müller cells (Fig. 3). We detected the protein in distinct intracellular structures resembling vesicles and multivesicular bodies. These structures were located in endfeet of Müller cells and in their radial processes apposed to the external limiting membrane (ELM) of the outer retina (Fig. 3). Interestingly, we also observed VAMP5-positive vesicle-like structures on the extracellular side of the internal limiting membrane facing the vitreous body and around apical microvilli of Müller cells reaching into the subretinal space surrounding photoreceptor segments (Fig. 3). Together, our ultrastructural observations revealed the presence of

VAMP5 in vesicular structures located in the cytoplasm of Müller cells and in the extracellular space facing the internal and external limiting membrane *in vivo*.

Presence of EV markers in specialized domains of retinal Müller cells

Our findings raised the question whether VAMP5 is associated with EVs secreted by Müller cells. To explore this, we studied the distribution of CD81 (TSPAN28), CD9 (TSPAN29) and CD63 (TSPAN30) in Müller cells. These transmembrane proteins are ubiquitously expressed members of the tetraspanin family, located in distinct cellular compartments and contained in distinct types of EVs (Escola et al., 1998; Théry et al., 1999; Théry et al., 2018). Immunohistochemical and -cytochemical detection of the selected tetraspanins in retinal sections (Fig. 4a) and in acutely isolated cells (Fig. 4b), respectively revealed a distinct distribution of each protein along GLUL-positive Müller cells. The cell surface component CD9 decorated their endfeet facing the vitreous body, structures in the outer plexiform layer and notably their apical microvilli extending into the subretinal space. CD81 was strongly expressed in the outer plexiform layer and on apical microvilli of Müller cells. CD63, which is also present in the endosomal-lysosomal system (Escola et al., 1998; Kobayashi et al., 2000; Pols and Klumperman, 2009), showed a distinct distribution: It was present in the endfeet of Müller cells and nearly absent from their apical microvilli (Fig. 4a). Inspection of acutely isolated Müller cells showed limited overlap of CD9 and CD81 and some colocalization of CD9 and CD63 (Fig. 4b). CD9 and CD63 also showed punctate staining non-associated with GLUL raising the question whether these proteins were expressed by other types of retinal cells. To address this question, we compared expression levels between retinal cell types using transcriptome (RNAseq) and proteome (mass spectrometry) analyses of affinity-purified cells (Fig. 5). For each tetraspanin tested, transcript and protein levels were highest in Müller cells compared to other cells with the notable exception of CD81,

which was also abundant in neurons (Fig. 5). Taken together, these results revealed a domain-specific presence of the selected tetraspanins with CD63 expressed on Müller cell endfeet facing the vitreous body, and CD9 and CD81 strongly present on apical microvilli of Müller cells extending into the subretinal space.

Ultrastructural and molecular characterization of EVs secreted by Müller cells *in vitro*

Our observations *in vivo* suggested that Müller cells secrete EVs. To characterize these structures, we purified Müller cells from retinal cell suspensions by immunomagnetic separation, cultured them for maximally 60h under chemically defined, serum-free conditions and prepared secreted material contained in CM as outlined below. For comparison, we also analysed material in CM of retinal neurons. To ensure survival of cells in defined medium during the indicated period, we first performed TUNEL assays. This approach revealed stable viability of GLUL-positive Müller cells, and only a slight decrease in the viability of GLUL-negative cells representing, in part, neurons (Fig. 6a). Next, we characterized material secreted by retinal Müller cells and neurons by established methods (Théry et al., 2018). As first step, we enriched material contained in Müller cell- and neuron-derived CM by ultracentrifugation and inspected the form and size of structures in these samples by SEM. Electron microscopic inspection revealed round, vesicle-like structures (Fig. 6b) with diameters between 30 to 150 nm (Fig. 6c, top panel), which is within the established size range of EVs. Independent information about the size of these structures was obtained by NTA, which also informed about particle concentrations (Fig. 6c, bottom panel). To this end, we enriched material secreted by Müller cells and neurons by immunomagnetic separation of CM using an antibody against CD9. These samples showed a narrower size range than the ultracentrifugation-enriched material inspected by SEM probably due to the affinity-based selection step (Fig. 6c). Notably, NTA revealed a ~1000-fold higher concentration of

particles in affinity-purified samples compared to CM thus indicating efficient enrichment of EV-like material (Fig. 6c, insert). We next probed whether Müller cells secrete VAMP5. To this end, we purified CD9-positive material from Müller cell-derived CM and subjected the lysate to immunoblotting. This approach revealed the presence of VAMP5 – albeit at low levels – in CD9-positive material secreted by Müller cells, but not in material secreted by neurons (Fig. 6d). To test directly whether VAMP5 is present on EV-like structures, we subjected CD9- and CD63-positive material secreted by cultured Müller cells to immunogold staining followed by SEM or TEM. Electron microscopic inspection revealed the presence of VAMP5 in CD9- and CD63-positive structures resembling EVs (Fig. 6e,f).

Distinct proteomic profiles of CD9- and CD63-positive EVs secreted by neurons and Müller cells *in vitro*

We next determined the protein composition of affinity-purified material secreted by cultured Müller cells and neurons using label-free mass spectrometry (Fig. 7). As controls, we analysed the protein content of non-binding flow-through of CM and of lysates of cultured and of acutely isolated cells, each from Müller cells and neurons (Fig. 7). The mass spectrometric data revealed an enrichment of established (CD9, CD81, ALIX, FLOT1, ANXA2) and of more specific EV components (COL1A2: Velázquez-Enríquez et al., 2021; LGALS3BP: Luga et al., 2012) in the CD9- and CD63-affinity purified samples compared to flow-through of media and to cell lysates (Fig. 7). On the other hand, proteins of organelles unrelated to EVs were only present in lysates, but absent from secreted material. This observation excluded the presence of contaminating material and indicated the quality of our EV preparations. Glial and neuronal markers were enriched in the respective lysates confirming their cell-specific origin (Fig. 7). Among these proteins, the cytoplasmic components GLUL and MAP1B were also present in material affinity-purified from CM

(Fig. 7). To explore the cell- and subtype-specific protein composition of presumed EVs, abundance values of proteins were subjected to hierarchical clustering (Fig. 8). The resulting sample clusters (columns) recapitulated the experimental groups indicating distinct compositions of neuron- and glia-secreted material and differences among CD9- and CD63-positive EV samples. The approach assigned proteins detected in EV samples (rows) to four principal groups (Fig. 8): Cluster 1 and cluster 2 contained either Müller cell- or and neuron-specific components, respectively. Two additional clusters contained proteins that were expressed in both neurons and Müller cells at high levels (Cluster 3) and at distinct levels (Cluster 4) across all experimental groups. Notably, all clusters contained EV components as shown by GO term analysis (Fig. 8). To further explore the diversity of glia- and neuron-derived EVs, we compared the protein contents of CD9- and CD63-positive material in CM from Müller cells and from neurons. As shown in Figure 9a, between 59% to 64% of proteins detected in EV-like structures secreted by Müller cells or neurons were non-overlapping and thus specific to the cell of origin. This fraction was similarly high in CD9- and CD63-positive material. This finding indicated that neurons and Müller cells secrete EVs with distinct protein contents. A comparison of proteins in CD9- and CD63-positive EVs from neurons revealed 80% overlap (Fig. 9b) indicating that the two subfractions of material secreted by neurons have a very similar protein content. Notably, this percentage was lower (60%) in material secreted by Müller cells, indicating that the CD9- and CD63-positive EVs secreted by these cells have more distinct compositions (Fig. 9b). A comparison of our proteomic data with entries in the Vesiclepedia database (Pathan et al., 2019) revealed that half of the proteins detected in neuron- and Müller cells-derived EVs are established markers (Fig. 9). Notably, we found CD81 and diazepam binding inhibitor (DBI) exclusively in CD9-positive EVs from Müller cells, whereas the fibrinogen beta chain (FGB) was only detected in their CD63-positive counterparts. The EV component galectin 3 binding protein (LGALS3BP)

was present in neuronal and Müller cell-derived CD9-positive EVs (Fig. 9). Among the new proteins strongly enriched in Müller-derived EVs are centrosomal protein 290 (CEP290) and carbonic anhydrase (CAR). Taken together, our findings revealed that affinity-purified Müller cells secrete EVs *in vitro* that have a distinct protein composition from those secreted by neurons. Moreover, CD9- and CD63-positive EVs from Müller cells show limited protein overlap indicating distinct subsets.

Colocalization of VAMP5 with tetraspanins in the extracellular space of the inner and outer retina *in vivo*

Our finding that VAMP5 and selected tetraspanins are present on EV-like material secreted by Müller cells *in vitro* prompted us to examine their colocalization on extracellular structures in retinae *in vivo* using light and electron microscopy. Immunohistochemical staining of retinal sections revealed overlapping distribution of VAMP5 with CD63 at Müller cell endfeet (Fig. 10a) and with CD9 in apical microvilli around photoreceptor segments (Fig. 10b). The apposition of CD63 and VAMP5 in Müller cell endfeet was corroborated by super-resolution light microscopy (Fig. 10c,d). The post-ischemic increase of VAMP5 expression (Fig. 2) prompted us to test whether induction of transient ischemia affected the colocalization of VAMP5 and the tetraspanin CD9. As shown in Fig. 11, ischemia induced time- and layer-dependent changes in the distribution of CD9 and VAMP5. CD9 showed a more increased presence on plasma membraness, especially in apical microvilli of Müller cells, whereas VAMP5 showed a more wide-spread expression in post-ischemic retinae (Fig. 11).

Our light microscopic observations indicated overlap of VAMP5 and the tetraspanins in specialized domains of Müller cells situated in the inner and outer retina, but we could not distinguish intra- and extracellular structures. To address this crucial point, we performed

immunogold labeling of respective proteins in ultrathin retinal sections. TEM inspection revealed close apposition of VAMP5 and CD63 in the extracellular space forming the vitreous body suggesting their presence on vesicle-like structures (Fig. 12a). Notably, we observed regularly vesicle-like structures decorated with VAMP5 and CD9 in the extracellular space intercalated between photoreceptor segments and Müller cell microvilli at variable distance from the external limiting membrane (Fig. 12b).

Discussion

Our study provides first evidence that Müller cells release distinct EV-like structures from specialized compartments in the inner and outer retina. Until now, EVs have mainly been studied after isolation from biological fluids or cell culture media. Here, we report their detection in an intact biological tissue *in vivo*, which has represented a key challenge in the field (van Niel et al., 2022; Verweij et al., 2021). Previously, EVs have been found in various ocular structures and fluids including acutely isolated retinae from mice (Mighty et al., 2020; Wooff et al., 2020), liquid biopsies of the human vitreous body (Zhao et al., 2018) and aqueous humor (Hsiao et al., 2021), the conjunctival mucin layer of rats (Tendler and Panshin, 2020), the RPE of aged mice (Wang et al., 2009) and drusen of patients with age-related macular degeneration (Grillo et al., 2021). However, the cellular origin of these EVs remained unclear. Our findings point to Müller cells as a major source of EVs and indicate that their release occurs at two prominent compartments of these cells. Müller cells are highly polarized showing distinct morphologic and functional specializations at their business ends: endfeet facing the vitreous body and apical microvilli surrounding photoreceptor segments (Derouiche et al., 2012; Reichenbach, 1989). Our results suggest that Müller cells secrete subsets of EVs from these compartments possibly by distinct mechanisms based on their tetraspanin content: The presence of CD63 in multivesicular bodies of endfeet and in the

apposed extracellular space suggests that EVs in this compartment originate from intraluminal vesicles. The presence of CD9 on EVs in the subretinal space suggests that these structures result from shedding of microvillar membranes. The presence of CD81 (Clarke and Geisert, 1998) and CD9 (Iwagawa et al., 2020) in Müller cell compartments of the inner and outer retina is supported by earlier reports. So far, the retinal distribution of CD63 has remained unknown. Here, we report its enrichment in Müller cell endfeet, and a low expression on microvilli in the outer retina. With respect to other retinal cells, this ubiquitously expressed tetraspanin has been studied in cultured human retinal pigment epithelial cells as part of their EVs (Sreekumar et al., 2010) and in rodent retinal ganglion cells as component of the endosomal-lysosomal system (Demais et al., 2016).

Until now, EVs secreted by primary Müller cells *in vitro* have not been characterized except for a recent report showing the presence of micro RNAs in these structures (Akamine et al., 2021). In fact, Müller cells have been mainly studied as target of EVs (Didiano et al., 2020; Eastlake et al., 2021; Kamalden et al., 2017; Ke et al., 2021; Peng et al., 2018; Wassmer et al., 2017; Zhang et al., 2020). Probably the best studied source of retinal EVs are cultured pigment epithelial cells (Ahn et al., 2021; Flores-Bellver et al., 2021; Kang et al., 2014; Klingeborn et al., 2017; Mukai et al., 2021; Otsuki et al., 2021; Sreekumar et al., 2010; Toyofuku et al., 2012). Few studies characterized EVs secreted by other types of retinal cells *in vitro* including precursor cells (Zhou et al., 2018), astrocytes (Hajrasouliha et al., 2013), retinal ganglion cells (Wang et al., 2021) and photoreceptors (Kalargyrou et al., 2021). Here, we provide the first direct comparison of neuronal and glial secretome. Our analysis reveals that Müller cells and retinal neurons secrete EVs with distinct protein compositions showing less than 40% overlap. Müller cell-specific EV components included DBI and FGB as well as carbonic anhydrase, which has been identified previously in Müller cells (Linser and Moscona, 1981; Ochrietor et al., 2005), and CEP290 (NPHP6), a ciliary component that has

not been associated with EVs, but whose deficiency causes retinal diseases (Chen et al., 2021). EVs secreted by cultured neurons (Chivet et al., 2014; Faure et al., 2006; Lachenal et al., 2011; Morel et al., 2013; Yuyama et al., 2012) and glial cells (Frühbeis et al., 2013; Gabrielli et al., 2015; Glebov et al., 2015; Guitart et al., 2016; Hooper et al., 2012; Potolicchio et al., 2005) from other parts of the CNS have been characterized, but their proteomic profiles have not been compared. Notably, the small overlap of proteins found in CD9- and CD63-positive EVs from Müller cells supports the notion that a given cell type produces distinct subtypes of EVs (Jeppesen et al., 2019; Kowal et al., 2016) and corroborates our idea that Müller cells secrete distinct types of EVs from distinct compartments, namely their basal endfeet and apical microvilli.

Our analysis of vesicle-associated membrane proteins revealed Müller cell-specific expression of VAMP5. Up to now, the distribution of this protein in the retina has remained unknown. Previous reports detected VAMP5 in skeletal muscle and other organs, but not in the brain (Takahashi et al., 2013; Zeng et al., 1998). A more recent study identified *Vamp5* as miRNA-regulated target gene in the retina indicating its presence in this part of the CNS (Olivares et al., 2017). Our finding that VAMP5 is associated with EVs is supported by several lines of evidence. Electron microscopic inspection of muscle cell lines revealed its localization at the plasma membrane, in vesicular structures and in multivesicular bodies (Tajika et al., 2014; Zeng et al., 1998) in line with our immunogold data. Moreover, VAMP5 was detected in EVs of the murine lung (Choudhary et al., 2021), from cultured myotubes (Forterre et al., 2014), mesenchymal stem cells (Salomon et al., 2013) and tumoral Jurkat T cells (Bosque et al., 2016). A hint towards the function of VAMP5 in EVs comes from a recent observation that components of the SNARE complex can be transferred intercellularly via EVs enabling vesicular release in target cells (Vilcaes et al., 2021). VAMP5 has also been shown to be part of the machinery that mediates EV-dependent cytokine release from

mesenchymal stem cells *in vitro* (Kou et al., 2018). VAMP5 did not mediate fusion of vesicular and plasma membrane containing specific tSNAREs in an artificial exocytosis assay (Hasan et al., 2010), but deletion of VAMP5 from mice causes developmental defects in the respiratory and urinary systems and perinatal death (Ikezawa et al., 2018). The observed upregulation of VAMP5 and the changes in CD9 distribution under ischemic conditions suggest that VAMP5 is part of the gliotic reaction to injury and disease and that ischemia affects EV secretion in the retina. Ischemia-induced changes in brain cells releasing EVs have been reported previously (Brenna et al., 2020). On the other hand, EVs are explored as therapeutic approaches to mitigate post-ischemic pathologic changes (Doeppner et al., 2015).

In summary, our data support the idea of EV-based communication between cells in the CNS and suggest Müller cells as a key actor in the retina.

Acknowledgements

Author contributions: VD: performed electron microscopy-related work, acquired and analysed electron micrographs. AP: performed immunofluorescence microscopy-related work, qPCR experiments and analyses, immunoblots for VAMP expression in the healthy and ischemic retina, established protocols for primary Müller cell cultures and performed EV purification. KW: performed EV purification from primary Müller cell cultures and immunoblot analyses, analyzed EV marker localization via STED microscopy. AMP: generated purified EVs for mass spectrometric analysis. LK: performed EV isolation and bioinformatic analysis of proteomic data. AB: performed immunohistochemical staining with selected antibodies to prepare immungold staining. RD: performed NTA. BP: set up the EV isolation protocol, analysed results, edited the manuscript. BG: analysed NTA results and edited the manuscript. SMH: performed mass spectrometric analysis of retinal cell types and

purified EVs, analysed protein expression levels and edited the manuscript. AG: designed experiments, analysed results, prepared figures and edited the manuscript. FWP: designed experiments, analysed results, prepared figures and wrote the manuscript. The authors thank Alexandra Hauser, Dirkje Felder and Gabrielle Jäger for excellent technical assistance.

Funding statement

Part of this work was supported by the Centre National de la Recherche Scientifique under grant UPR3212 (FWP), the Université de Strasbourg under grant UPR3212 (FWP), the Agence National de la Recherche Scientifique under grant GLIAVAMP (FWP), the Deutsche Forschungsgemeinschaft under grants GR 4403/1-1; GR 4403/5-1; GR 4403/7-1 (AG) and HA 6014/5-1 (SMH) and the ProRetina Foundation Germany under grants Pro-Re/Seed/Grosche.1-2014 (AG) and Pro-Re/Seed/Kaplan-Grosche.1-2019 (LK, AG).

Declaration of Interest Statement

The authors report no conflict of interest

Data Availability Statement

Data are available on request from the authors

References

Ahn JY et al. (2021) Release of extracellular vesicle miR-494-3p by ARPE-19 cells with impaired mitochondria. Biochimica et Biophysica Acta (BBA) - General Subjects 1865:129598. https://doi.org/https://doi.org/10.1016/j.bbagen.2020.129598.

Aires ID et al. (2021) Microglial Extracellular Vesicles as Vehicles for Neurodegeneration Spreading. Biomolecules 11:770. https://doi.org/10.3390/biom11060770.

Akamine PS et al. (2021) Age-related increase of let-7 family microRNA in rat retina and vitreous. Exp Eye Res 204:108434. https://doi.org/https://doi.org/10.1016/j.exer.2020.108434.

Araujo APB, Carpi-Santos R, Gomes FCA (2019) The Role of Astrocytes in the Development of the Cerebellum. Cerebellum 18:1017-1035. https://doi.org/10.1007/s12311-019-01046-0.

Bosque A et al. (2016) Comparative proteomics of exosomes secreted by tumoral Jurkat T cells and normal human T cell blasts unravels a potential tumorigenic role for valosin-containing protein. Oncotarget 7:29287-29305. https://doi.org/10.18632/oncotarget.8678.

Brenna S et al. (2020) Characterization of brain-derived extracellular vesicles reveals changes in cellular origin after stroke and enrichment of the prion protein with a potential role in cellular uptake. J Extracell Vesicles 9:1809065-1809065. https://doi.org/10.1080/20013078.2020.1809065.

Brenna S, Krisp C, Altmeppen HC, Magnus T, Puig B (2021) Brain-Derived Extracellular Vesicles in Health and Disease: A Methodological Perspective. Int J Mol Sci 22:1365.

Budnik V, Ruiz-Cañada C, Wendler F (2016) Extracellular vesicles round off communication in the nervous system. Nat Rev Neurosci 17:160-172. https://doi.org/10.1038/nrn.2015.29.

Chen HY, Kelley RA, Li T, Swaroop A (2021) Primary cilia biogenesis and associated retinal ciliopathies. Semin Cell Dev Biol 110:70-88. https://doi.org/https://doi.org/10.1016/j.semcdb.2020.07.013.

Chivet M et al. (2014) Exosomes secreted by cortical neurons upon glutamatergic synapse activation specifically interact with neurons. J Extracell Vesicles 3:24722. https://doi.org/http://doi.org/10.3402/jev.v3.24722.

Choudhary I et al. (2021) Vesicular and extravesicular protein analyses from the airspaces of ozone-exposed mice revealed signatures associated with mucoinflammatory lung disease. Sci Rep 11:23203-23203. https://doi.org/10.1038/s41598-021-02256-5.

Clarke K, Geisert EE, Jr. (1998) The target of the antiproliferative antibody (TAPA) in the normal and injured rat retina. Mol Vis 4:3.

Demais V et al. (2016) Reversal of Pathologic Lipid Accumulation in NPC1-Deficient Neurons by Drug-Promoted Release of LAMP1-Coated Lamellar Inclusions. J Neurosci 36:8012-8025. https://doi.org/10.1523/jneurosci.0900-16.2016.

Derouiche A et al. (2012) Beyond polarity: functional membrane domains in astrocytes and Muller cells. Neurochem Res 37:2513-2523.

Didiano D et al. (2020) Induction of a proliferative response in the zebrafish retina by injection of extracellular vesicles. Exp Eye Res 200:108254-108254. https://doi.org/10.1016/j.exer.2020.108254.

Doeppner TR et al. (2015) Extracellular Vesicles Improve Post-Stroke Neuroregeneration and Prevent Postischemic Immunosuppression. Stem Cells Transl Med 4:1131-1143. https://doi.org/10.5966/sctm.2015-0078.

Dragovic RA et al. (2011) Sizing and phenotyping of cellular vesicles using Nanoparticle Tracking Analysis. Nanomedicine : nanotechnology, biology, and medicine 7:780-788. https://doi.org/10.1016/j.nano.2011.04.003.

Eastlake K et al. (2021) Prospects for the application of Müller glia and their derivatives in retinal regenerative therapies. Prog Retin Eye Res 85:100970. https://doi.org/https://doi.org/10.1016/j.preteyeres.2021.100970.

Escartin C et al. (2021) Reactive astrocyte nomenclature, definitions, and future directions. Nat Neurosci. https://doi.org/10.1038/s41593-020-00783-4.

Escola J-M et al. (1998) Selective Enrichment of Tetraspan Proteins on the Internal Vesicles of Multivesicular Endosomes and on Exosomes Secreted by Human B-lymphocytes. J Biol Chem 273:20121-20127. https://doi.org/https://doi.org/10.1074/jbc.273.32.20121.

Faure J et al. (2006) Exosomes are released by cultured cortical neurones. Mol Cell Neurosci 31:642-648. https://doi.org/10.1016/j.mcn.2005.12.003.

Fiacco TA, McCarthy KD (2018) Multiple Lines of Evidence Indicate That Gliotransmission Does Not Occur under Physiological Conditions. J Neurosci 38:3-13. https://doi.org/10.1523/jneurosci.0016-17.2017.

Flores-Bellver M et al. (2021) Extracellular vesicles released by human retinal pigment epithelium mediate increased polarised secretion of drusen proteins in response to AMD stressors. J Extracell Vesicles 10:e12165-e12165. https://doi.org/10.1002/jev2.12165.

Forterre A et al. (2014) Proteomic analysis of C2C12 myoblast and myotube exosome-like vesicles: a new paradigm for myoblast-myotube cross talk? PLoS ONE 9:e84153-e84153. https://doi.org/10.1371/journal.pone.0084153.

Frühbeis C et al. (2013) Neurotransmitter-triggered transfer of exosomes mediates oligodendrocyte-neuron communication. Plos Biology 11:e1001604-e1001604. https://doi.org/10.1371/journal.pbio.1001604.

Gabrielli M et al. (2015) Active endocannabinoids are secreted on extracellular membrane vesicles. EMBO Rep 16:213-220. https://doi.org/http://doi.org/10.15252/embr.201439668.

García-Cáceres C et al. (2019) Role of astrocytes, microglia, and tanycytes in brain control of systemic metabolism. Nat Neurosci 22:7-14. https://doi.org/10.1038/s41593-018-0286-y.

Giaume C, Naus CC, Sáez JC, Leybaert L (2021) Glial Connexins and Pannexins in the Healthy and Diseased Brain. Physiol Rev 101:93-145. https://doi.org/10.1152/physrev.00043.2018.

Glebov K et al. (2015) Serotonin stimulates secretion of exosomes from microglia cells. GLIA 63:626-634. https://doi.org/https://doi.org/10.1002/glia.22772.

Görgens A et al. (2019) Optimisation of imaging flow cytometry for the analysis of single extracellular vesicles by using fluorescence-tagged vesicles as biological reference material. J Extracell Vesicles 8:1587567-1587567. https://doi.org/10.1080/20013078.2019.1587567.

Grillo SL et al. (2021) Descriptive analysis of Fibulin-3 and the extracellular vesicle marker, Alix, in drusen from a small cohort of postmortem human eyes. Exp Eye Res 203:108422. https://doi.org/https://doi.org/10.1016/j.exer.2020.108422.

Grosche A et al. (2016) The Proteome of Native Adult Müller Glial Cells From Murine Retina. Mol Cell Proteomics 15:462-480. https://doi.org/https://doi.org/10.1074/mcp.M115.052183.

Guitart K et al. (2016) Improvement of neuronal cell survival by astrocyte-derived exosomes under hypoxic and ischemic conditions depends on prion protein. GLIA 64:896-910. https://doi.org/https://doi.org/10.1002/glia.22963.

Hajrasouliha AR et al. (2013) Exosomes from retinal astrocytes contain antiangiogenic components that inhibit laser-induced choroidal neovascularization. J Biol Chem 288:28058-28067. https://doi.org/10.1074/jbc.M113.470765.

Hasan N, Corbin D, Hu C (2010) Fusogenic pairings of vesicle-associated membrane proteins (VAMPs) and plasma membrane t-SNAREs--VAMP5 as the exception. PLoS ONE 5:e14238-e14238. https://doi.org/10.1371/journal.pone.0014238.

Hillen AEJ, Burbach JPH, Hol EM (2018) Cell adhesion and matricellular support by astrocytes of the tripartite synapse. Prog Neurobiol 165-167:66-86. https://doi.org/https://doi.org/10.1016/j.pneurobio.2018.02.002.

Hooper C et al. (2012) Wnt3a induces exosome secretion from primary cultured rat microglia. BMC Neurosci 13:144-144. https://doi.org/10.1186/1471-2202-13-144.

Hsiao Y-P et al. (2021) Differences in the Quantity and Composition of Extracellular Vesicles in the Aqueous Humor of Patients with Retinal Neovascular Diseases. Diagnostics (Basel, Switzerland) 11:1276. https://doi.org/10.3390/diagnostics11071276.

Ikezawa M et al. (2018) Loss of VAMP5 in mice results in duplication of the ureter and insufficient expansion of the lung. Dev Dyn 247:754-762. https://doi.org/10.1002/dvdy.24618.

Illes P, Burnstock G, Tang Y (2019) Astroglia-Derived ATP Modulates CNS Neuronal Circuits. Trends Neurosci 42:885-898. https://doi.org/https://doi.org/10.1016/j.tins.2019.09.006.

Iwagawa T et al. (2020) Cd9 Protects Photoreceptors from Injury and Potentiates Edn2 Expression. Invest Ophthalmol Vis Sci 61:7. https://doi.org/10.1167/iovs.61.3.7.

Jeppesen DK et al. (2019) Reassessment of Exosome Composition. Cell 177:428-+. https://doi.org/10.1016/j.cell.2019.02.029.

Jha MK, Morrison BM (2020) Lactate Transporters Mediate Glia-Neuron Metabolic Crosstalk in Homeostasis and Disease. Front Cell Neurosci 14. https://doi.org/10.3389/fncel.2020.589582.

Kalargyrou AA et al. (2021) Nanotube-like processes facilitate material transfer between photoreceptors. EMBO Rep 22:e53732-e53732. https://doi.org/10.15252/embr.202153732.

Käll L, Canterbury JD, Weston J, Noble WS, MacCoss MJ (2007) Semi-supervised learning for peptide identification from shotgun proteomics datasets. Nature Methods 4:923-925. https://doi.org/10.1038/nmeth1113.

Kalluri R, LeBleu VS (2020) The biology, function, and biomedical applications of exosomes. Science 367:640-+. https://doi.org/10.1126/science.aau6977.

Kamalden TA et al. (2017) Exosomal MicroRNA-15a Transfer from the Pancreas Augments Diabetic Complications by Inducing Oxidative Stress. Antioxidants & redox signaling 27:913-930. https://doi.org/10.1089/ars.2016.6844.

Kang GY et al. (2014) Exosomal proteins in the aqueous humor as novel biomarkers in patients with neovascular age-related macular degeneration. J Proteome Res 13:581-595. https://doi.org/10.1021/pr400751k.

Ke Y et al. (2021) Human embryonic stem cell-derived extracellular vesicles alleviate retinal degeneration by upregulating Oct4 to promote retinal Müller cell retrodifferentiation via HSP90. Stem cell research & therapy 12:21-21. https://doi.org/10.1186/s13287-020-02034-6.

Kim D, Langmead B, Salzberg SL (2015) HISAT: a fast spliced aligner with low memory requirements. Nat Methods 12:357-360. https://doi.org/10.1038/nmeth.3317.

Kim YS, Choi J, Yoon B-E (2020) Neuron-Glia Interactions in Neurodevelopmental Disorders. Cells 9:2176. https://doi.org/10.3390/cells9102176.

Klingeborn M et al. (2017) Directional Exosome Proteomes Reflect Polarity-Specific Functions in Retinal Pigmented Epithelium Monolayers. Sci Rep 7:4901. https://doi.org/10.1038/s41598-017-05102-9.

Kobayashi T et al. (2000) The tetraspanin CD63/lamp3 cycles between endocytic and secretory compartments in human endothelial cells. Mol Biol Cell 11:1829-1843. https://doi.org/10.1091/mbc.11.5.1829.

Kofuji P, Araque A (2021) Astrocytes and Behavior. Annu Rev Neurosci. https://doi.org/10.1146/annurev-neuro-101920-112225.

Kou X et al. (2018) The Fas/Fap-1/Cav-1 complex regulates IL-1RA secretion in mesenchymal stem cells to accelerate wound healing. Sci Transl Med 10:eaai8524. https://doi.org/10.1126/scitranslmed.aai8524.

Kowal J et al. (2016) Proteomic comparison defines novel markers to characterize heterogeneous populations of extracellular vesicle subtypes. Proc Natl Acad Sci U S A 113:E968-E977. https://doi.org/10.1073/pnas.1521230113.

Lachenal G et al. (2011) Release of exosomes from differentiated neurons and its regulation by synaptic glutamatergic activity. Mol Cell Neurosci 46:409-418. https://doi.org/https://doi.org/10.1016/j.mcn.2010.11.004.

Lago-Baldaia I, Fernandes VM, Ackerman SD (2020) More Than Mortar: Glia as Architects of Nervous System Development and Disease. Front Cell Dev Biol 8:611269. https://doi.org/10.3389/fcell.2020.611269.

Langmead B, Trapnell C, Pop M, Salzberg SL (2009) Ultrafast and memory-efficient alignment of short DNA sequences to the human genome. Genome Biology 10:R25. https://doi.org/10.1186/gb-2009-10-3-r25.

Li H et al. (2019) Glia-derived exosomes: Promising therapeutic targets. Life Sci 239:116951. https://doi.org/https://doi.org/10.1016/j.lfs.2019.116951.

Linnerbauer M, Wheeler MA, Quintana FJ (2020) Astrocyte Crosstalk in CNS Inflammation. Neuron 108:608-622. https://doi.org/10.1016/j.neuron.2020.08.012.

Linser P, Moscona AA (1981) Carbonic anhydrase C in the neural retina: transition from generalized to glia-specific cell localization during embryonic development. Proc Natl Acad Sci U S A 78:7190-7194. https://doi.org/10.1073/pnas.78.11.7190.

Liu J et al. (2020) Roles of Exosomes in Ocular Diseases. International journal of nanomedicine 15:10519-10538. https://doi.org/10.2147/IJN.S277190.

Lizarraga-Valderrama LR, Sheridan GK (2021) Extracellular vesicles and intercellular communication in the central nervous system. FEBS Letters 595:1391-1410. https://doi.org/https://doi.org/10.1002/1873-3468.14074.

Luga V et al. (2012) Exosomes Mediate Stromal Mobilization of Autocrine Wnt-PCP Signaling in Breast Cancer Cell Migration. Cell 151:1542-1556. https://doi.org/https://doi.org/10.1016/j.cell.2012.11.024.

Martin M (2011) Cutadapt removes adapter sequences from high-throughput sequencing reads. EMBnetjournal 17:10-12.

Mathieu M, Martin-Jaular L, Lavieu G, Thery C (2019) Specificities of secretion and uptake of exosomes and other extracellular vesicles for cell-to-cell communication. Nat Cell Biol 21:9-17. https://doi.org/10.1038/s41556-018-0250-9.

Mighty J et al. (2020) Analysis of Adult Neural Retina Extracellular Vesicle Release, RNA Transport and Proteomic Cargo. Invest Ophthalmol Vis Sci 61:30. https://doi.org/10.1167/iovs.61.2.30.

Morel L et al. (2013) Neuronal Exosomal miRNA-dependent Translational Regulation of Astroglial Glutamate Transporter GLT1. J Biol Chem 288:7105-7116. https://doi.org/https://doi.org/10.1074/jbc.M112.410944.

Mukai A et al. (2021) Mitochondrial miRNA494-3p in extracellular vesicles participates in cellular interplay of iPS-Derived human retinal pigment epithelium with macrophages. Exp Eye Res 208:108621. https://doi.org/https://doi.org/10.1016/j.exer.2021.108621.

Murat CDB, García-Cáceres C (2021) Astrocyte Gliotransmission in the Regulation of Systemic Metabolism. Metabolites 11:732. https://doi.org/10.3390/metabo11110732.

Nave KA, Werner HB (2021) Ensheathment and Myelination of Axons: Evolution of Glial Functions. Annu Rev Neurosci. https://doi.org/10.1146/annurev-neuro-100120-122621.

Ochrietor JD et al. (2005) Carbonic anhydrase XIV identified as the membrane CA in mouse retina: strong expression in Müller cells and the RPE. Exp Eye Res 81:492-500. https://doi.org/https://doi.org/10.1016/j.exer.2005.03.010.

Olivares AM et al. (2017) Multimodal Regulation Orchestrates Normal and Complex Disease States in the Retina. Sci Rep 7:690-690. https://doi.org/10.1038/s41598-017-00788-3.

Otsuki Y et al. (2021) CD63+ extracellular vesicles from retinal pigment epithelial cells participate in crosstalk with macrophages in the innate inflammatory axis. Experimental Eye Research 205:108496. https://doi.org/https://doi.org/10.1016/j.exer.2021.108496.

Pannicke T et al. (2014) Differential effects of P2Y1 deletion on glial activation and survival of photoreceptors and amacrine cells in the ischemic mouse retina. Cell Death Dis 5:e1353. https://doi.org/10.1038/cddis.2014.317.

Pascual M, Ibáñez F, Guerri C (2020) Exosomes as mediators of neuron-glia communication in neuroinflammation. Neural regeneration research 15:796-801. https://doi.org/10.4103/1673-5374.268893.

Patel DC, Tewari BP, Chaunsali L, Sontheimer H (2019) Neuron-glia interactions in the pathophysiology of epilepsy. Nat Rev Neurosci 20:282-297. https://doi.org/10.1038/s41583-019-0126-4.

Pathan M et al. (2019) Vesiclepedia 2019: a compendium of RNA, proteins, lipids and metabolites in extracellular vesicles. Nucleic Acids Res 47:D516-D519. https://doi.org/10.1093/nar/gky1029.

Pauly D et al. (2019) Cell-Type-Specific Complement Expression in the Healthy and Diseased Retina. Cell Rep 29:2835-2848.e2834. https://doi.org/10.1016/j.celrep.2019.10.084.

Pekny M et al. (2016) Astrocytes: a central element in neurological diseases. Acta Neuropathol 131:323-345. https://doi.org/10.1007/s00401-015-1513-1.

Peng Y et al. (2018) Human embryonic stem cells extracellular vesicles and their effects on immortalized human retinal Müller cells. PLoS ONE 13:e0194004-e0194004. https://doi.org/10.1371/journal.pone.0194004.

Pertea M et al. (2015) StringTie enables improved reconstruction of a transcriptome from RNA-seq reads. Nat Biotechnol 33:290-295. https://doi.org/10.1038/nbt.3122.

Pfrieger FW, Vitale N (2018) Cholesterol and the journey of extracellular vesicles. J Lipid Res 59:2255-2261. https://doi.org/10.1194/jlr.R084210.

Pistono C, Bister N, Stanová I, Malm T (2020) Glia-Derived Extracellular Vesicles: Role in Central Nervous System Communication in Health and Disease. Front Cell Dev Biol 8:623771. https://doi.org/10.3389/fcell.2020.623771.

Pols MS, Klumperman J (2009) Trafficking and function of the tetraspanin CD63. Exp Cell Res 315:1584-1592.

Potolicchio I et al. (2005) Proteomic Analysis of Microglia-Derived Exosomes: Metabolic Role of the Aminopeptidase CD13 in Neuropeptide Catabolism. J Immunol 175:2237-2243. https://doi.org/10.4049/jimmunol.175.4.2237.

Raiders S et al. (2021) Engulfed by Glia: Glial Pruning in Development, Function, and Injury across Species. J Neurosci 41:823-833. https://doi.org/10.1523/jneurosci.1660-20.2020.

Raudvere U et al. (2019) g:Profiler: a web server for functional enrichment analysis and conversions of gene lists (2019 update). Nucleic Acids Res 47:W191-W198. https://doi.org/10.1093/nar/gkz369.

Reichenbach A (1989) Attempt to classify glial cells by means of their process specialization using the rabbit retinal Müller cell as an example of cytotopographic specialization of glial cells. GLIA 2:250-259. https://doi.org/10.1002/glia.440020406.

Reichenbach A, Bringmann A (2020) Glia of the human retina. GLIA 68:768-796. https://doi.org/10.1002/glia.23727.

Salomon C et al. (2013) Exosomal signaling during hypoxia mediates microvascular endothelial cell migration and vasculogenesis. PLoS ONE 8:e68451-e68451. https://doi.org/10.1371/journal.pone.0068451.

Savtchouk I, Volterra A (2018) Gliotransmission: Beyond Black-and-White. J Neurosci 38:14-25. https://doi.org/10.1523/JNEUROSCI.0017-17.2017.

Schäfer N, Grosche A, Schmitt SI, Braunger BM, Pauly D (2017) Complement Components Showed a Time-Dependent Local Expression Pattern in Constant and Acute White Light-Induced Photoreceptor Damage. Front Mol Neurosci 10:197. https://doi.org/10.3389/fnmol.2017.00197.

Schindelin J et al. (2012) Fiji: an open-source platform for biological-image analysis. Nat Methods 9:676-682. https://doi.org/10.1038/nmeth.2019.

Schnatz A, Müller C, Brahmer A, Krämer-Albers E-M (2021) Extracellular Vesicles in neural cell interaction and CNS homeostasis. FASEB bioAdvances 3:577-592. https://doi.org/10.1096/fba.2021-00035.

Seifert G, Steinhäuser C (2018) Heterogeneity and function of hippocampal macroglia. Cell Tissue Res 373:653-670. https://doi.org/10.1007/s00441-017-2746-1.

Sharma P, Schiapparelli L, Cline HT (2013) Exosomes function in cell-cell communication during brain circuit development. Curr Opin Neurobiol 23:997-1004. https://doi.org/10.1016/j.conb.2013.08.005.

Shen WD, Nikolic L, Meunier C, Pfrieger F, Audinat E (2017) An autocrine purinergic signaling controls astrocyte-induced neuronal excitation. Sci Rep 7. https://doi.org/10.1038/s41598-017-11793-x.

Slezak M et al. (2012) Relevance of exocytotic glutamate release from retinal glia. Neuron 74:504-516.

Sokolova V et al. (2011) Characterisation of exosomes derived from human cells by nanoparticle tracking analysis and scanning electron microscopy. Colloids Surf B Biointerfaces 87:146-150. https://doi.org/https://doi.org/10.1016/j.colsurfb.2011.05.013.

Sreekumar PG et al. (2010) αB crystallin is apically secreted within exosomes by polarized human retinal pigment epithelium and provides neuroprotection to adjacent cells. PLoS ONE 5:e12578. https://doi.org/http://doi.org/10.1371/journal.pone.0012578.

Südhof TC, Rothman JE (2009) Membrane fusion: grappling with SNARE and SM proteins. Science 323:474-477. https://doi.org/10.1126/science.1161748.

Sultan S et al. (2015) Synaptic Integration of Adult-Born Hippocampal Neurons Is Locally Controlled by Astrocytes. Neuron 88:957-972. https://doi.org/10.1016/j.neuron.2015.10.037.

Tajika Y et al. (2014) Vesicular transport system in myotubes: ultrastructural study and signposting with vesicle-associated membrane proteins. Histochem Cell Biol 141:441-454. https://doi.org/10.1007/s00418-013-1164-z.

Takahashi M et al. (2013) The localization of VAMP5 in skeletal and cardiac muscle. Histochemistry and Cell Biology 139:573-582. https://doi.org/http://doi.org/10.1007/s00418-012-1050-0.

Tan CX, Burrus Lane CJ, Eroglu C (2021) Role of astrocytes in synapse formation and maturation. Curr Top Dev Biol 142:371-407. https://doi.org/10.1016/bs.ctdb.2020.12.010.

Team RC (2021). https://www.R-project.org/.

Tendler Y, Panshin A (2020) Features of p53 protein distribution in the corneal epithelium and corneal tear film. Sci Rep 10:10051-10051. https://doi.org/10.1038/s41598-020-67206-z.

Théry C et al. (1999) Molecular Characterization of Dendritic Cell-Derived Exosomes: Selective Accumulation of the Heat Shock Protein Hsc73. J Cell Biol 147:599-610. https://doi.org/10.1083/jcb.147.3.599.

Théry C et al. (2018) Minimal information for studies of extracellular vesicles 2018 (MISEV2018): a position statement of the International Society for Extracellular Vesicles and update of the MISEV2014 guidelines. J Extracell Vesicles 7:1535750. https://doi.org/10.1080/20013078.2018.1535750.

Toyofuku T et al. (2012) Endosomal sorting by Semaphorin 4A in retinal pigment epithelium supports photoreceptor survival. Genes Dev 26:816-829. https://doi.org/10.1101/gad.184481.111.

Trapnell C, Pachter L, Salzberg SL (2009) TopHat: discovering splice junctions with RNA-Seq. Bioinformatics 25:1105-1111. https://doi.org/10.1093/bioinformatics/btp120.

Urbina FL, Gupton SL (2020) SNARE-Mediated Exocytosis in Neuronal Development. Front Mol Neurosci 13:133-133. https://doi.org/10.3389/fnmol.2020.00133.

van Niel G et al. (2022) Challenges and directions in studying cell–cell communication by extracellular vesicles. Nat Rev Mol Cell Biol. https://doi.org/10.1038/s41580-022-00460-3.

Vardjan N, Parpura V, Verkhratsky A, Zorec R (2019) Gliocrine System: Astroglia as Secretory Cells of the CNS. Advances in experimental medicine and biology 1175:93-115. https://doi.org/10.1007/978-981-13-9913-8_4.

Velázquez-Enríquez JM et al. (2021) Proteomic Analysis Reveals Key Proteins in Extracellular Vesicles Cargo Associated with Idiopathic Pulmonary Fibrosis In Vitro. Biomedicines 9:1058. https://doi.org/10.3390/biomedicines9081058.

Verweij FJ et al. (2021) The power of imaging to understand extracellular vesicle biology in vivo. Nat Methods 18:1013-1026. https://doi.org/10.1038/s41592-021-01206-3.

Vilcaes AA, Chanaday NL, Kavalali ET (2021) Interneuronal exchange and functional integration of synaptobrevin via extracellular vesicles. Neuron 109:971-983.e975. https://doi.org/10.1016/j.neuron.2021.01.007.

Wagner L et al. (2016) Effects of IP3R2 Receptor Deletion in the Ischemic Mouse Retina. Neurochem Res 41:677-686. https://doi.org/10.1007/s11064-015-1735-6.

Wagner L et al. (2017) Suppression of SNARE-dependent exocytosis in retinal glial cells and its effect on ischemia-induced neurodegeneration. GLIA. https://doi.org/10.1002/glia.23144.

Wang AL et al. (2009) Autophagy and exosomes in the aged retinal pigment epithelium: possible relevance to drusen formation and age-related macular degeneration. PLoS ONE 4:e4160-e4160. https://doi.org/10.1371/journal.pone.0004160.

Wang T et al. (2021) Exosome-Mediated Delivery of the Neuroprotective Peptide PACAP38 Promotes Retinal Ganglion Cell Survival and Axon Regeneration in Rats With

Traumatic Optic Neuropathy. Front Cell Dev Biol 9:659783-659783. https://doi.org/10.3389/fcell.2021.659783.

Wassmer SJ, Carvalho LS, György B, Vandenberghe LH, Maguire CA (2017) Exosome-associated AAV2 vector mediates robust gene delivery into the murine retina upon intravitreal injection. Sci Rep 7:45329-45329. https://doi.org/10.1038/srep45329.

Wilton DK, Dissing-Olesen L, Stevens B (2019) Neuron-Glia Signaling in Synapse Elimination. Annu Rev Neurosci 42:107-127. https://doi.org/10.1146/annurev-neuro-070918-050306.

Wilton DK, Stevens B (2020) The contribution of glial cells to Huntington's disease pathogenesis. Neurobiol Dis 143:104963. https://doi.org/10.1016/j.nbd.2020.104963.

Wiśniewski JR, Zougman A, Nagaraj N, Mann M (2009) Universal sample preparation method for proteome analysis. Nat Methods 6:359-362. https://doi.org/10.1038/nmeth.1322.

Wooff Y et al. (2020) Small-Medium Extracellular Vesicles and Their miRNA Cargo in Retinal Health and Degeneration: Mediators of Homeostasis, and Vehicles for Targeted Gene Therapy. Front Cell Neurosci 14:160-160. https://doi.org/10.3389/fncel.2020.00160.

Yates AG et al. (2022) In sickness and in health: The functional role of extracellular vesicles in physiology and pathology in vivo. J Extracell Vesicles 11:e12151. https://doi.org/https://doi.org/10.1002/jev2.12151.

You Y, Ikezu T (2019) Emerging roles of extracellular vesicles in neurodegenerative disorders. Neurobiol Dis 130:104512. https://doi.org/https://doi.org/10.1016/j.nbd.2019.104512.

Yuyama K, Sun H, Mitsutake S, Igarashi Y (2012) Sphingolipid-modulated Exosome Secretion Promotes Clearance of Amyloid-β by Microglia. J Biol Chem 287:10977-10989. https://doi.org/https://doi.org/10.1074/jbc.M111.324616.

Zamanian JL et al. (2012) Genomic analysis of reactive astrogliosis. J Neurosci 32:6391-6410. https://doi.org/10.1523/jneurosci.6221-11.2012.

Zeng Q et al. (1998) A novel synaptobrevin/VAMP homologous protein (VAMP5) is increased during in vitro myogenesis and present in the plasma membrane. Mol Biol Cell 9:2423-2437. https://doi.org/10.1091/mbc.9.9.2423.

Zhang W, Jiang H, Kong Y (2020) Exosomes derived from platelet-rich plasma activate YAP and promote the fibrogenic activity of Müller cells via the PI3K/Akt pathway. Exp Eye Res 193:107973. https://doi.org/https://doi.org/10.1016/j.exer.2020.107973.

Zhao Y et al. (2018) Liquid Biopsy of Vitreous Reveals an Abundant Vesicle Population Consistent With the Size and Morphology of Exosomes. Translational vision science & technology 7:6-6. https://doi.org/10.1167/tvst.7.3.6.

Zhou J et al. (2018) Retinal progenitor cells release extracellular vesicles containing developmental transcription factors, microRNA and membrane proteins. Sci Rep 8:2823-2823. https://doi.org/10.1038/s41598-018-20421-1.

Figures

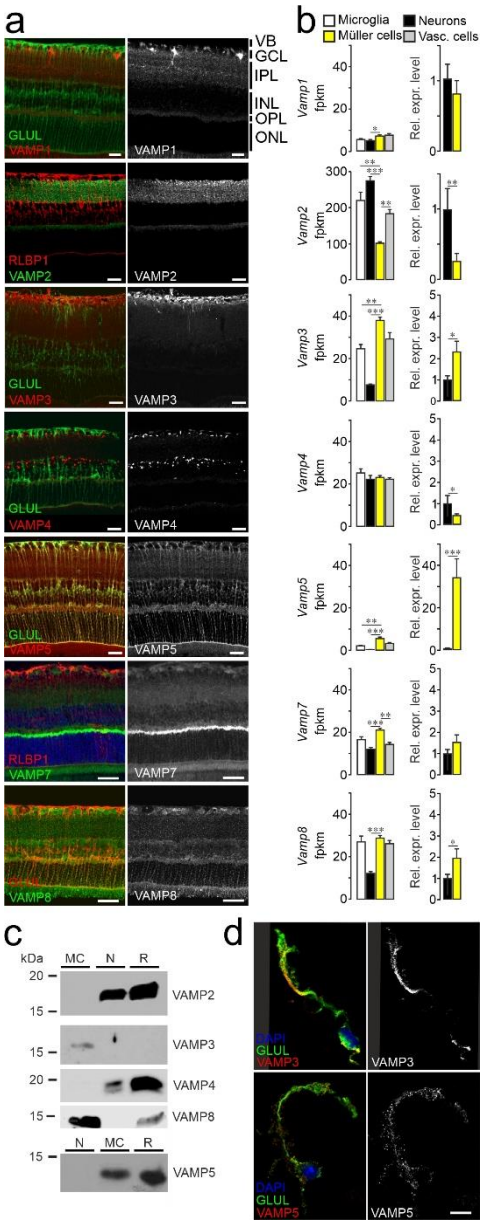

Figure 1. Expression of VAMP3, 5 and 8 by retinal Müller cells.

(a) False-color and grayscale confocal micrographs of retinal sections from adult mice subjected to immunohistochemical staining of the indicated VAMPs and of the Müller cell markers GLUL and RLBP1. Scale bars: 20 µm. VB, vitreous body; GCL, ganglion cell layer; IPL, inner plexiform layer; INL, inner nuclear layer; OPL, outer plexiform layer; ONL, outer nuclear layer. (b) Left, average transcript counts of indicated *Vamps* obtained by RNAseq from lysates of indicated types of acutely isolated affinity-purified retinal cells (n = 3-4

preparations; Mann-Whitney test; whiskers indicate SEM). Fpkm, fragments per kilobase million. Right, mean relative expression levels of indicated *Vamps* in Müller cells compared to neurons. (c) Representative immunoblots showing the presence of selected VAMPs in indicated populations of acutely isolated cells (MC, Müller cells; N, neurons; R, whole retinal extracts). For each protein tested, equal amounts of total protein from indicated samples were loaded. (d) False-color and grey-scale micrographs of acutely isolated Müller cells subjected to nuclear (blue) and immunocytochemical staining of VAMP3 and VAMP5 (red) and GLUL (green). Scale bar: 10 µm.

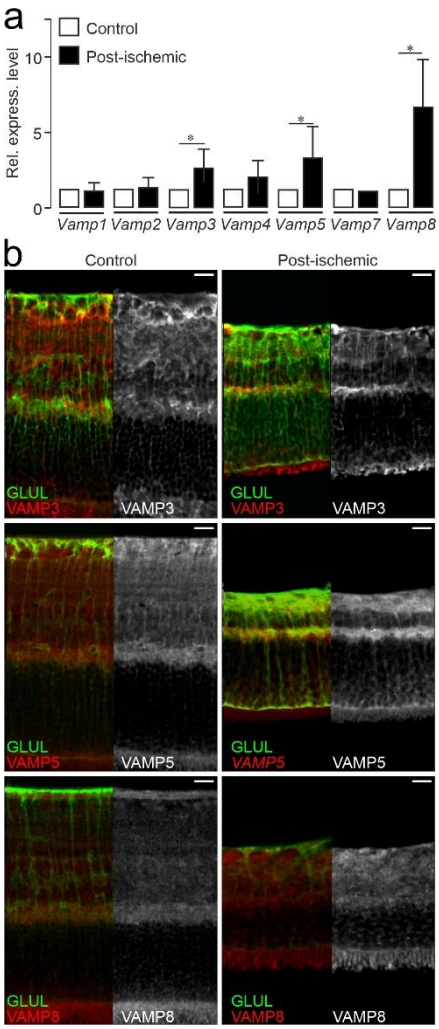

Figure 2. Ischemia-induced increase of *Vamp3*, *Vamp5* and *Vamp8* expression in retinal Müller cells.

(a) Average relative levels of indicated transcripts as determined by qRT-PCR in acutely isolated affinity purified Müller cells from retinae at 7 days after transient ischemia (post-ischemic). Levels were normalized to those in Müller cells isolated from untreated control eyes (n = 3 preparations; whiskers indicate SEM; Mann-Whitney test). (b) False-color and gray-scale confocal micrographs of retinal sections from control eyes and from eyes at 7 days after transient ischemia followed by immunohistochemical staining of the indicated VAMPs (red) and of GLUL-positive Müller cells (green). Scale bar: 20 µm

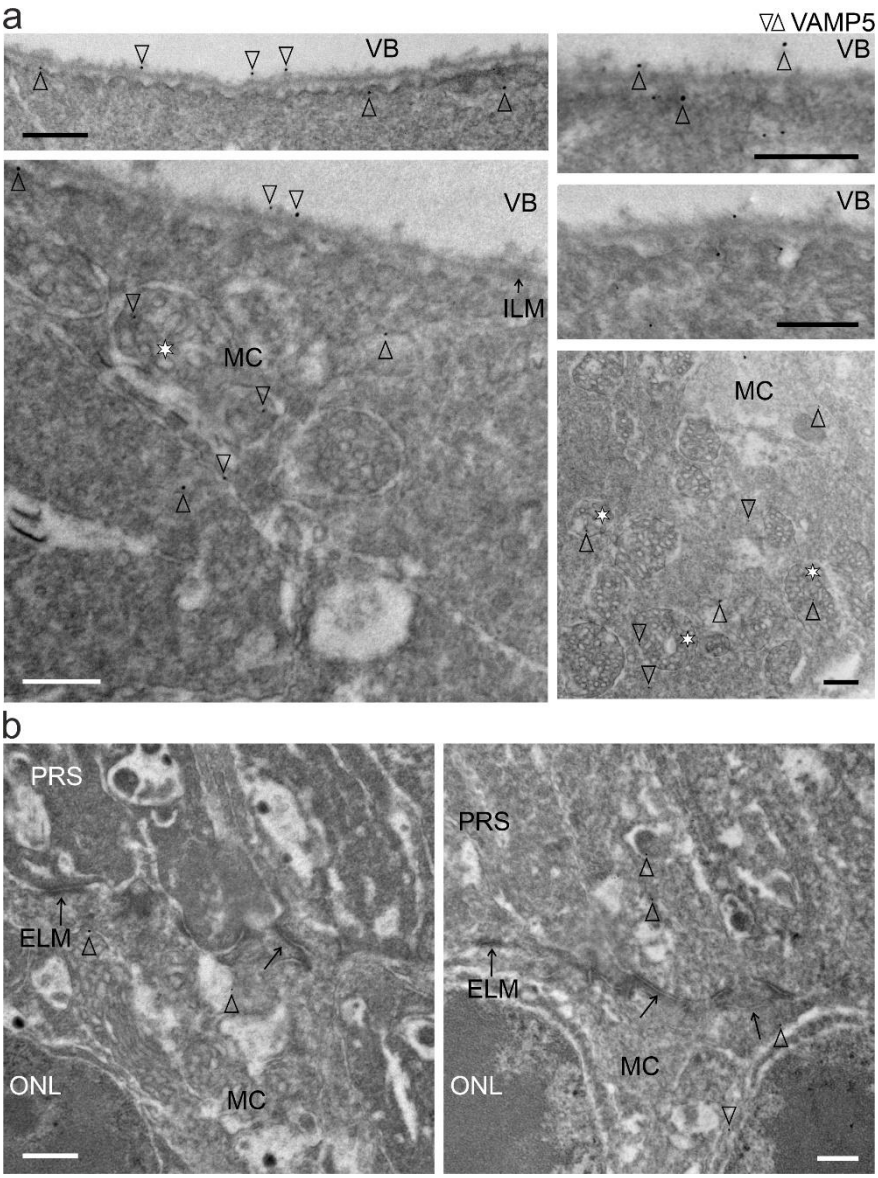

Figure 3. Subcellular and extracellular location of VAMP5 in the retina.

(a) Transmission electron micrographs of the inner retina showing the presence of VAMP5 (empty arrowheads) in endfeet of Müller cells (MC), notably in multivesicular bodies (asterisks), at the intra- and extracellular side of the internal limiting membrane (ILM) and in the vitreous body (VB). (b) Electron micrographs of the outer retina showing the presence of VAMP5 in processes of Müller cells in the outer nuclear layer (ONL) and on their apical microvilli extending beyond the external limiting membrane (ELM, black arrows) into the subretinal space containing photoreceptor segments (PRS). Retinal sections were subjected to

immunogold labeling of VAMP5. Selected nanogold particles are indicated by arrowheads. Scale bars: 500 nm.

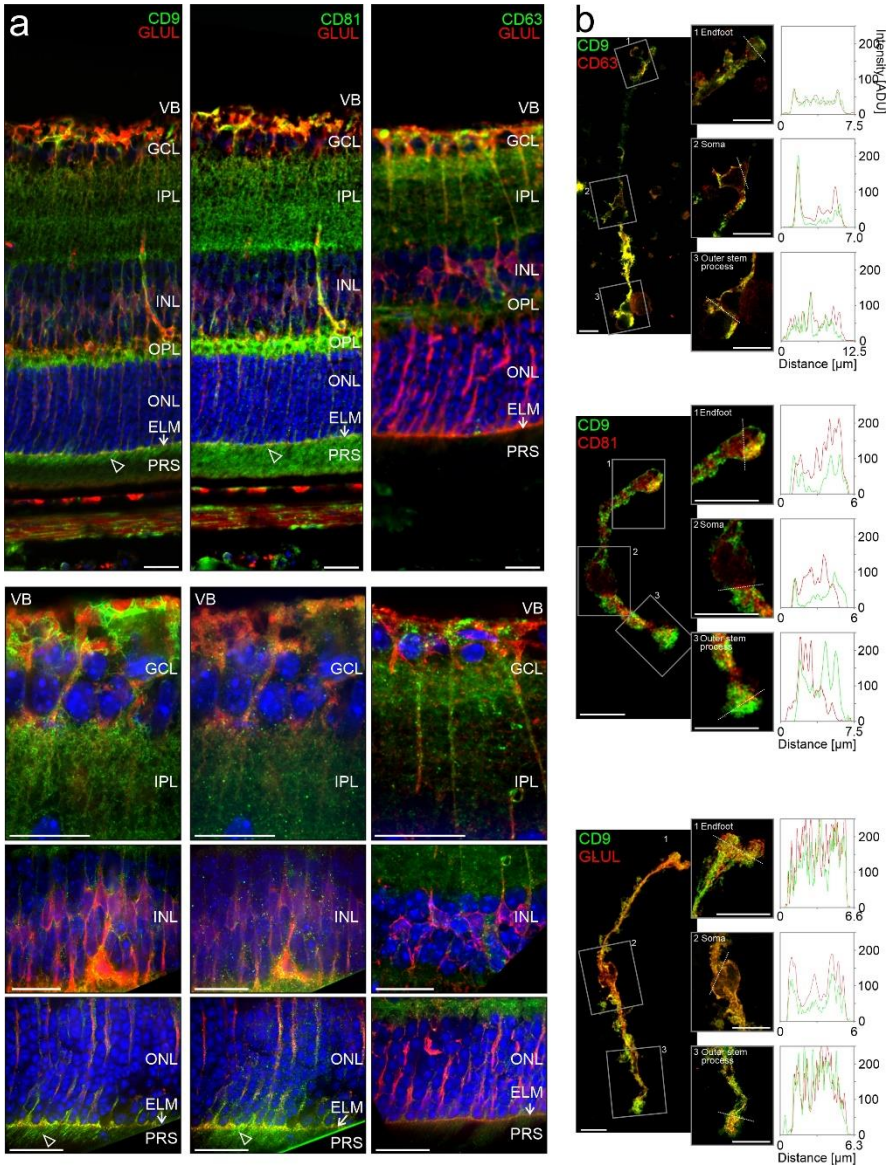

Figure 4. Distribution of EV markers in the retina.

(a) False-color confocal micrographs of retinal sections subjected to immunohistochemical staining of GLUL-positive retinal Müller cells and of the tetraspanins CD9, CD81 and CD63. Arrowheads indicate presence of CD9 and CD81 in microvilli extending in the subretinal space containing photoreceptor segments. Scale bars: 20 µm. VB, vitreous body; GCL, ganglion cell layer; IPL, inner plexiform layer; INL, inner nuclear layer; OPL, outer plexiform layer; ONL, outer nuclear layer; ELM, external limiting membrane (white arrows); PRS, photoreceptor segments; RPE, retinal pigment epithelium. (b) False-color confocal (left) and STED (right) micrographs of acutely isolated Müller cells showing entire cells and

selected compartments, indicated by rectangles, at higher magnification. The terms "endfoot" and "outer stem process" indicate the Müller cell compartments that are apposed to the internal and external limiting membrane in the intact retina, respectively. Fixed cells were subjected to immunocytochemical staining of CD9, CD63, CD81 and GLUL. Scale bars: 10 µm. Plots show fluorescence staining intensities of respective proteins across the selected compartments with the location of the line scans indicated by white dashed lines.

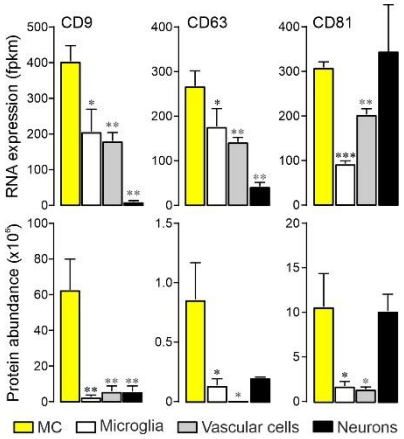

Figure 5. Cell-specific expression of tetraspanins in selected retinal cells.

Transcript (top) and protein levels (bottom) of indicated tetraspanins in affinity-purified retinal cells (n = 3-5; whiskers: SEM; Mann-Whitney test) as determined by RNAseq and mass spectrometry, respectively. Fpkm, fragments per kilobase million. MC, Müller cells.

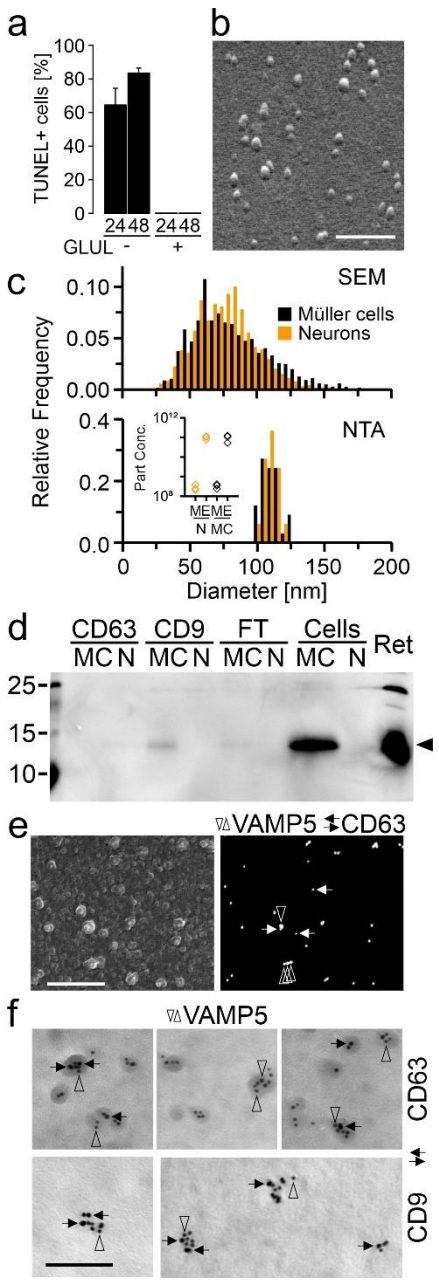

Figure 6. Characterization of EVs secreted by Müller cells *in vitro*.

(a) Viability of glutamine synthase (GLUL)-positive Müller cells and GLUL-negative neurons after indicated periods (in hours) in serum-free culture estimated by TUNEL staining. (b) Scanning electron micrograph of vesicle-like structures enriched by ultracentrifugation of culture medium from Müller cells. Scale bar: 600 nm. (c) Diameters of vesicle-like structures shown in (b) as determined by SEM (top; n = 3091 / 2361 particles from neurons / Müller cells; n = 3 culture preparations each; 10 images each preparation) and of CD9-positive EVs determined by NTA (bottom; n = 3 independent cultures). Orange and

black bars indicate neuronal and glia-derived material, respectively. Insert, particle concentration per mL in medium (M) and affinity-purified EVs (E) from neurons (N) and glial cells (MC). (d) Immunoblots probing the presence of VAMP5 in CD63- or CD9-positive EVs from cultured Müller cells (MC) and neurons (N), in the flow-through (FT), in cell lysates (Cells) and in the retina (Ret). (e) Scanning electron micrographs of secondary (left) and backscatter electrons (right) showing the surface and proteins, respectively of affinity-purified EVs from cultured Müller cells subjected to immunogold labeling of VAMP5 (vertical arrowheads) and CD63 (horizontal arrows). Scale bar: 750 nm. (f) Transmission electron micrographs showing colocalization of indicated proteins on affinity-purified EVs secreted by Müller cells *in vitro*. Sections were subjected to immunogold labeling of VAMP5 (vertical arrowheads) and CD63 or CD9 (horizontal arrows). Scale bar: 100 nm.

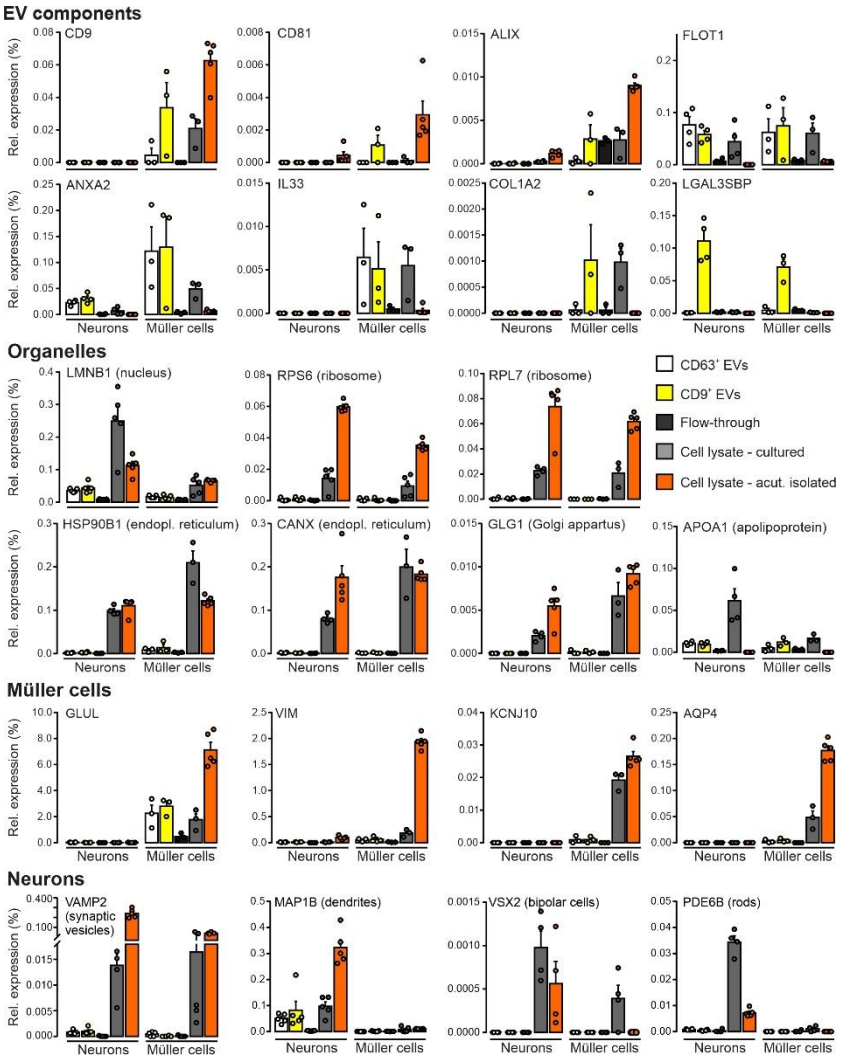

Figure 7. Presence of established markers in EVs secreted by Müller cells and neurons *in vitro*.

Relative expression levels of selected proteins contained in EVs, organelles, Müller cells and neurons in CD9- and CD63-positive EVs, in material of the flow-through, and in lysates of cultured and of acutely isolated neurons and Müller cells. Protein levels were normalized to total abundance of protein detected in respective samples. Symbols represent individual preparations. Bars and whiskers represent average values and SEM, respectively (n = 5 preparations).

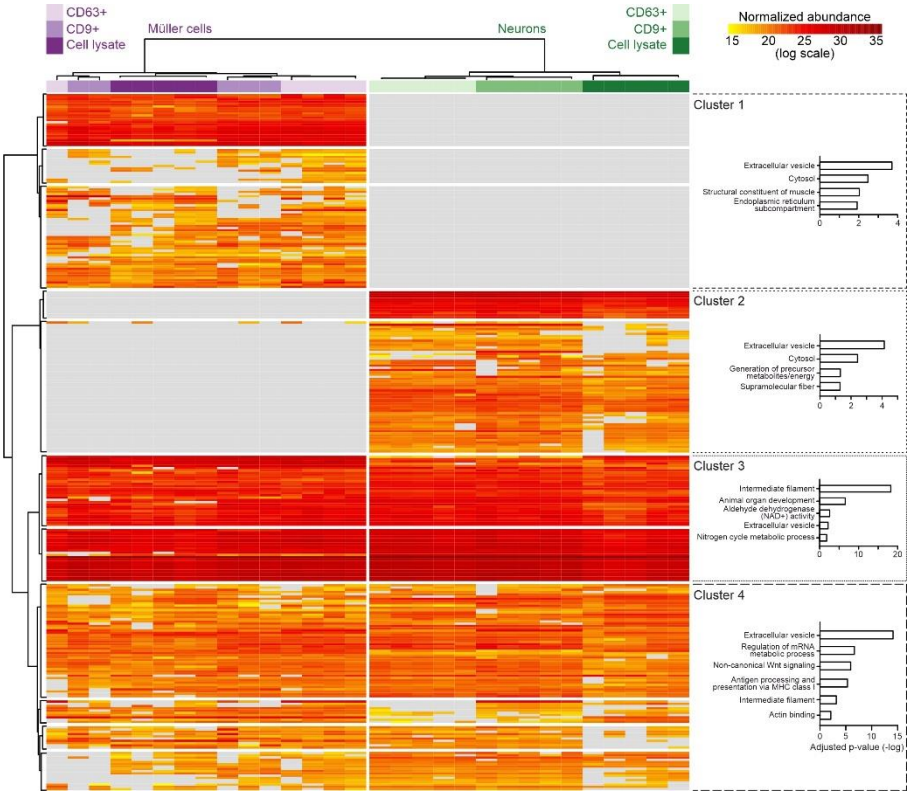

Figure 8. Protein profiles of CD9- and CD63-positive EVs from Müller cells and neurons.

Heatmap showing the normalized abundances of proteins detected in EVs by mass spectrometry and dendrograms showing grouping of columns (experimental conditions) and rows (proteins) generated by unsupervised hierarchical clustering. Plots on the right show GO terms in four largest protein clusters and respective adjusted p values.

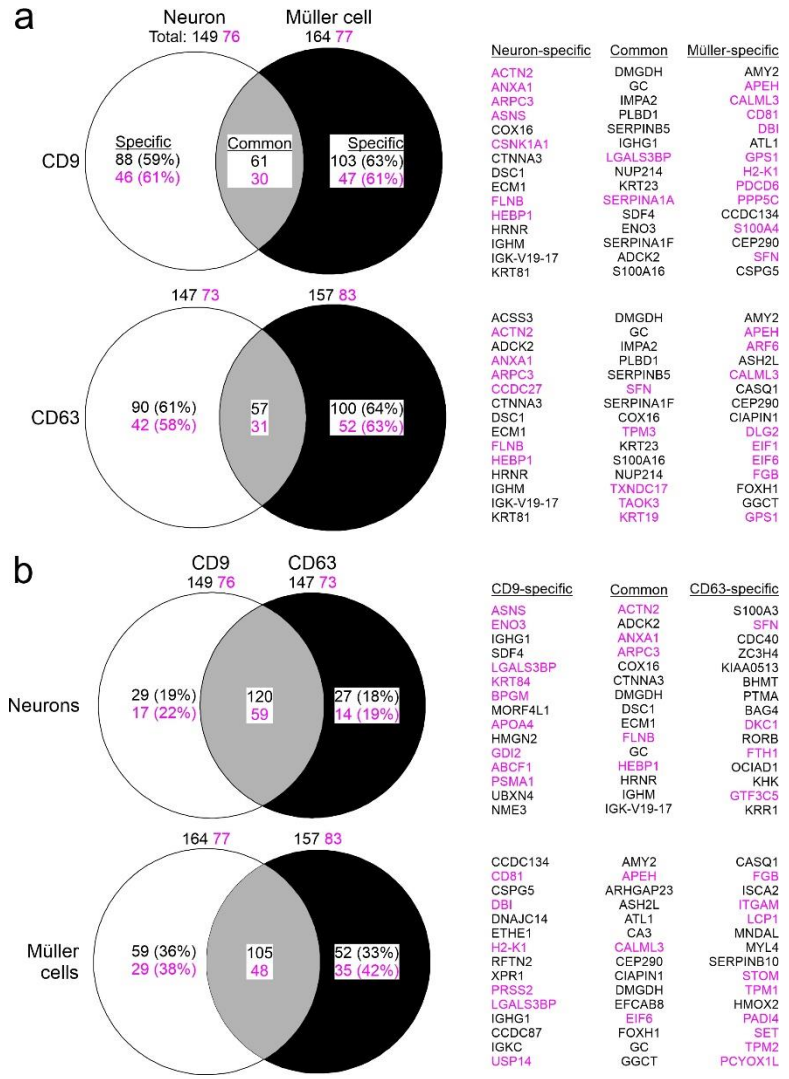

Figure 9. Diversity of neuron- and Müller cell-derived EVs based on protein content. Venn diagrams showing differences and overlaps in protein content between neurons and Müller cells for CD9- (top) and CD63-positive (bottom) EVs (a) and between CD9- and CD63-positive EVs from neurons (top) and from Müller cells (bottom) (b). Numbers indicate counts of all proteins that were detected in respective samples (total), that were present in both samples (common) and that were only present in either sample (specific). Indicated percentages were calculated compared to total number of detected proteins. Names of specific and common proteins showing highest enrichment in EVs compared to lysate (top 15) are indicated on the right. Numbers and names in magenta highlight established EV components listed in the Vesiclepedia database.

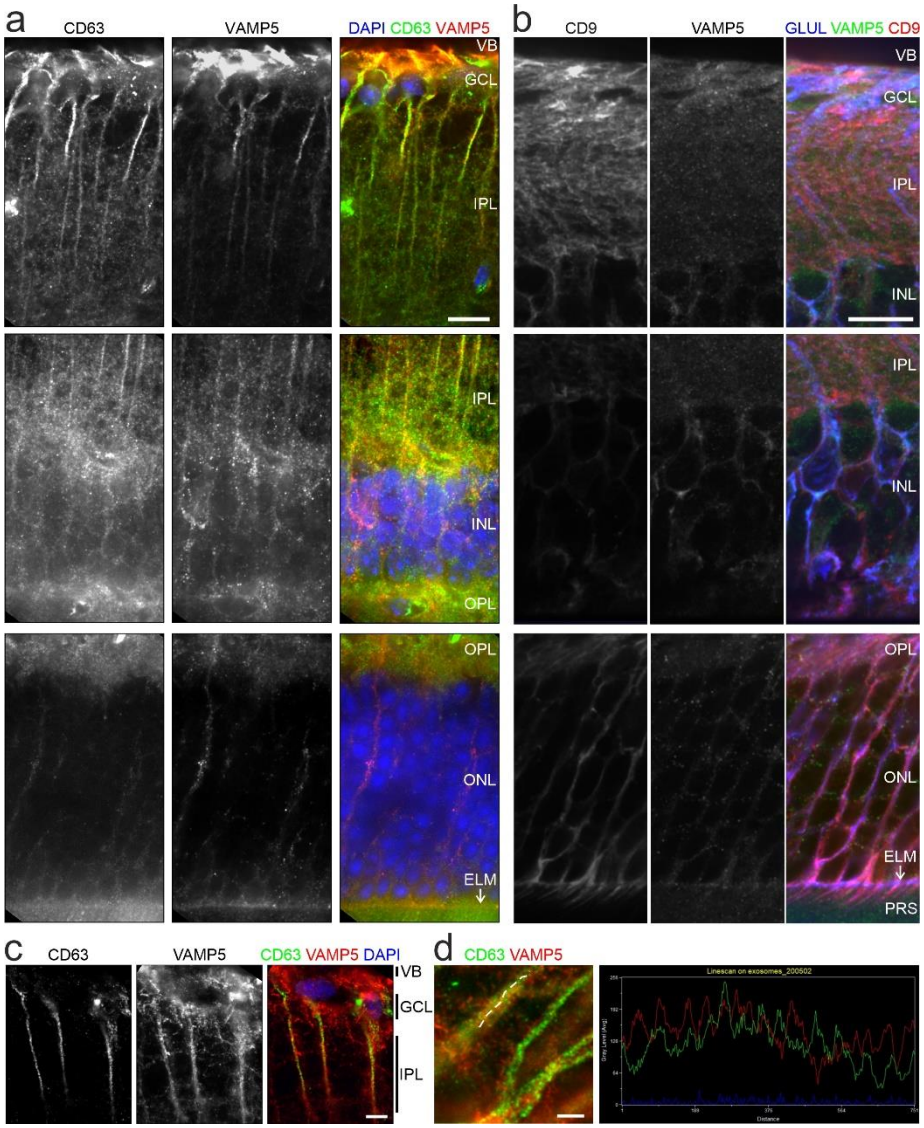

Figure 10. Colocalization of VAMP5 and EV markers in retinal cells *in vivo*.

Greyscale and false-color confocal micrographs of retinal sections subjected to immunohistochemical staining of VAMP5 and of CD63 (a) and CD9 (b). Scale bars: 10 µm. ELM, external limiting membrane (white arrows); GCL, ganglion cell layer; INL, inner nuclear layer; IPL, inner plexiform layer; ONL, outer nuclear layer; OPL, outer plexiform layer; PRS, photoreceptor segments; VB, vitreous body. (c) Greyscale and false-color STED micrographs of retinal sections after immunohistochemical staining of CD63 and VAMP5. Scale bar: 5 µm. (d) STED micrographs at higher magnification showing Müller cell processes (left). Plot of fluorescence intensities along the line scan indicated in the micrograph (dashed white line) (right). Scale bar: 5 µm.

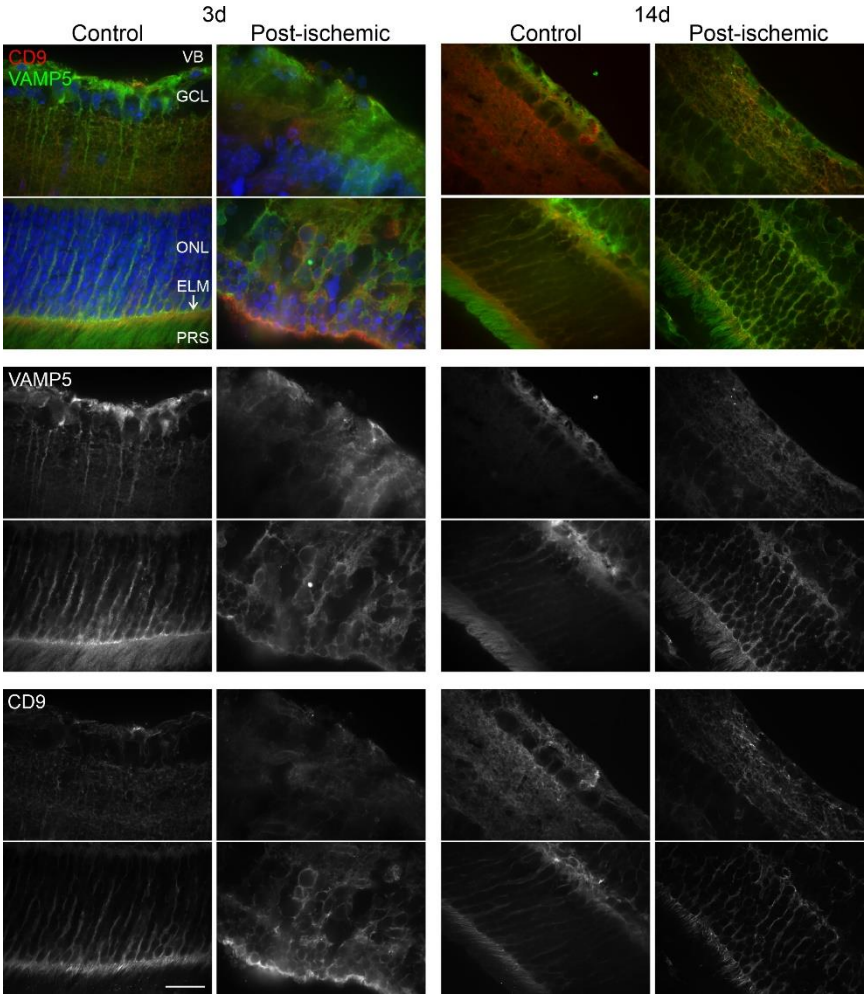

Figure 11. Post-ischemic changes in the retinal distribution of VAMP5 and CD9.

False-color and greyscale confocal micrographs of retinal sections subjected to immunohistochemical staining of VAMP5 and of CD9 at indicated days following induction of transient ischemia. Scale bar: 40 µm. ELM, external limiting membrane (white arrow); GCL, ganglion cell layer; ONL, outer nuclear layer; PRS, photoreceptor segments; VB, vitreous body.

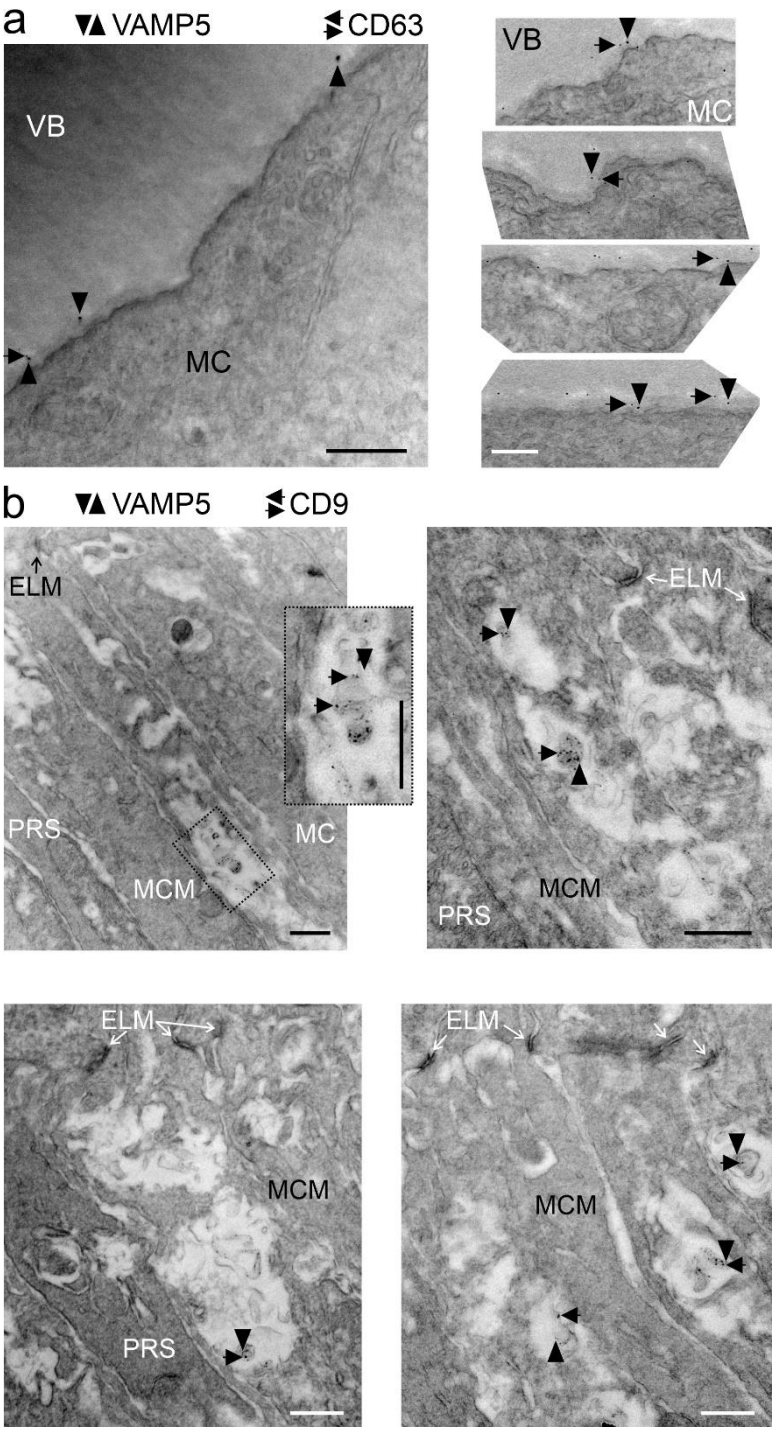

Figure 12. Colocalization of tetraspanins and VAMP5 on extracellular vesicular structures in the retina.

Representative transmission electron micrographs of retinal sections revealing colocalization of CD63 (a) and of CD9 (b) with VAMP5 in the extracellular space (a) apposed to endfeet forming the vitreous body and (b) close to microvilli of Müller cells surrounding

photoreceptor segments, respectively. Retinal ultrathin sections were subjected to immunogold labeling of the indicated proteins. ELM, external limiting membrane; MCM, Müller cell microvillus; PRS, photoreceptor segment; VB, vitreous body. VAMP5: vertical arrowheads; CD63 and CD9: horizontal arrows. Scale bars: 500 nm.

Supplementary table 1. Primary and secondary antibodies.

Primary antibodies				
Target	**Host**	**Company**	**Reference**	**Dilution**
GLUL	mouse	Merck (Darmstadt, Germany)	MAB302	1:1000 (IF)
CRALBP	rabbit	Santa Cruz (Dallas, USA)	sc-28193	1 : 200 (IF)
VAMP1	rabbit	Synaptic Systems (Göttingen, Germany)	104 002	1 : 100 (IF) 1 : 5000 (WB)
VAMP2	mouse	Synaptic Systems	104 211	1 : 100 (IF) 1 : 5000 (WB)
VAMP3	rabbit	Synaptic Systems	104 103	1 : 100 (IF) 1 : 5000 (WB)
VAMP4	rabbit	Thermofisher Scientific (Schwerte, Germany)	PA1-768	1 : 100 (IF) 1 : 5000 (WB)
VAMP5	rabbit	Synaptic Systems	176 003	1 : 100 (IF) 1 : 5000 (WB) 1: 100 (EM)
VAMP7	mouse	Synaptic Systems	232 011	1 : 500 (IF) 1 : 5000 (WB)

VAMP8	rabbit	Synaptic Systems	104 302	1 : 100 (IF) 1 : 5000 (WB)
CD9	rat	BD Biosciences (Heidelberg, Germany)	553758	1 : 100 (IF) 1 : 500 (WB) 1 : 50 (EM)
CD63	mouse	Abcam (Cambridge, UK)	ab108950	1 : 100 (IF) 1 : 1000 (WB) 1 : 50 (EM)
CD81	rabbit	Cell Signaling Technology (Frankfurt, Germany)	10037	1 : 100 (IF)

Secondary antibodies				
Target	**Host**	**Company**	**Reference**	**Dilution**
Rabbit IgG- HRP	goat	Merck Millipore (Darmstadt, Germany)	401315	1:10000
Mouse IgG Ig-HRP	goat	Merck Millipore (Darmstadt, Germany)	401215	1:10000
Rabbit IgG	donkey	Thermofisher Scientific	A-21206	1:500
Rat IgG	goat	Abberior (Göttingen, Germany)	2-0132-005-1	1 : 200
Mouse IgG	goat	Abberior	2-0002-005-1	1 : 200

Rat IgG- 10 nm gold particles	goat	Electron Microscopy Sciences/Euromedex, Souffelweyersheim, France	25189	1:100
Goat IgG – 15 nm gold particles	Donkey	Electron Microscopy Sciences	25807	1:100
Goat IgG – ultrasmall gold particles	Donkey	Electron Microscopy Sciences	25801	1:100
Rabbit IgG - 6 nm gold particles	Goat	Electron Microscopy Sciences	25363	1:100
Rabbit IgG - ultrasmall gold particles	Goat	Electron Microscopy Sciences	25412	1:100

Supplementary table 2. Primer and TaqMan probe combinations for the detection of VAMPs by qRT-PCR.

Gene ID	**Primer Sequences: *forward***	**Primer Sequences: *reverse***	**Roche TaqMan® Probe**
Vamp1	5‘ acg gac ctc cac ttc ctc tt 3‘	5‘ cag ctc ctt ctg tcc ctt ca 3‘	# 78
Vamp2	5‘ cca agc tca agc gca aat 3‘	5‘ggg att taa gtg ctg aag taa acg 3‘	# 31
Vamp3	5‘ttg aaa caa gtg ctg cca ag 3‘	5‘ atc cct atc gcc cac atc t 3‘	# 31
Vamp4	5‘tgc aag aga ata tta caa agg taa ttg 3‘	5‘ gaa agc ggt ggc att atc c 3‘	# 91
Vamp5	5‘ gag ttg gag cag cgt tca g 3‘	5‘ tgg gct aaa gtc ttg gtt gtc 3‘	# 17
Vamp7	5‘ gac ctt cgc ccc tca gtc 3‘	5‘ aga atg gcc atg act tca atc t 3‘	# 78
Vamp8	5‘ cct ccg aaa caa gac aga gg 3‘	5‘ gga caa tca cac aga tga tga ca 3‘	# 31